AN ABSTRACT OF THE THESIS OF

Nicholas D. Frederick for the degree of Master of Science in Chemical Engineering presented on June 28, 1985.

Title: Plain and Finned Tube Scaling in a Deluged Dry Cooling System.

Abstract approved: Redacted for Privacy

Dr. James G. Knudsen

Scaling characteristics on plain and finned tubes in a deluged dry cooling system were investigated. For all runs in this study drying and deluge times were held constant at 10 and 5 minutes respectively, water flow was 350 ml/min, and air velocity past the test section was 1.1 m/s. Simulated cooling tower water containing various corrosion inhibitor additives, and city water were used as delugates. Heat fluxes of 41.12, 49.34, 57.56 w/dm^2 were used.

Scaling on the plain tube test section was confined mainly to the lower half of the horizontal tube. End effects may have enhanced scale formation near the tube ends. Results suggest an asymptotic deposit might be reached, but more data are needed to verify this.

Scaling on the horizontal finned tube was confined mainly to the lower fin ridges, and the bottom base and fin faces. Asymptotic deposit values of 93 g/dm^2 at 49.34 w/dm^2, and 199 g/dm^2 at 57.56 w/dm^2 were observed.

The finned tube test section was found to scale at a much faster rate than the plain tube test section. There was better heat transfer on the finned tube under drying conditions, while the plain tube had better heat transfer under deluged conditions.

The data were fitted to four different two parameter equations. A modified Kern-Seaton deposit removal type equation,

$$m = m^{*} (1 - \exp(-C/\theta_{c}))$$

was found to fit the simulated cooling water runs best over the number of cycles studies.

When city water was used as a delugate corrosion on the heat transfer surface occurred. The amount of deposition was found to be proportional to the number of deluge cycles.

Plain and Finned Tube Scaling in a Deluged Dry Cooling System

by

Nicholas D. Frederick

A THESIS

submitted to

Oregon State University

in partial fulfillment of
the requirements for the
degree of

Master of Science

Completed June 28, 1985

Commencement June 1986

APPROVED:

Redacted for Privacy

Professor of Chemical Engineering in charge of major

Redacted for Privacy

Chairman of Chemical Engineering Department

Redacted for Privacy

Dean of Graduate School

Date thesis is presented June 28, 1985

Typed by Meredith Turton for Nicholas D. Frederick

ACKNOWLEGEMENTS

Many thanks to Dr. Knudsen for his help in all parts of this study. Thanks also to Mr. Nick Wannenmacher for his assistance with the experimental equipment. In addition, I would like to thank the Department of Chemical Engineering at Oregon State for monetary support, and for providing a solid education.

TABLE OF CONTENTS

LIST OF FIGURES

LIST OF TABLES

PLAIN AND FINNED TUBE SCALING IN A DELUGED DRY COOLING SYSTEM

CHAPTER I

INTRODUCTION

Fouling or scaling of heat exchangers is a common problem in cooling water systems. Fouling can be defined as the deposition of a thermally insulating material onto a heat transfer surface. Crystals, silt, corrosion products, biological growths, or a combination of these are all potential foulants.

In a deluged dry cooling tower system, waste heat from a condenser is transferred to the ambient air via an intermediate heat transfer fluid, such as water or ammonia, in a closed system. During the cool periods of the year, the system operates as an air cooled system. During the warm periods of the year the tower efficiency drops, hence there is a need to enhance the heat transfer process. This can be accomplished by deluging the outside of the heat exchange surface with water (7, 18). This type of system is advantageous in locations where cooling water is scarce.

One of the concerns in the operation of a deluged dry cooling tower is the deposition of solids from the delugate onto the heat exchange surface. This scaling can occur by two mechanisms (7):

1. Exceeding the solubility limits under continuous flow conditions.
2. Evaporation of the delugate on the heat exchange surface in multiple wet to dry cycles.

Important parameters in this scaling phenomenon are water chemistry, delugate temperature, surface temperature, number and duration of cycles, and flow characteristics on the outside of the heat transfer surface.

Scaling on both plain and finned tubes was studied in the present investigation. The mass of scale deposited as a function of number of deluge cycles for two different heat fluxes was determined. Simulated cooling tower water and city water were used as delugates.

CHAPTER II

GENERAL INFORMATION

Heat exchanger fouling is the accumulation of undesired solid material on a heat transfer surface. This solid film adds an additional resistance to heat transfer and thereby lowers the efficiency of the heat exchanger. Fouling can be classified into six distinguishable categories as follows (4):

1. Precipitation fouling or scaling — the crystalization of inverse solubility salts onto a heated surface that is above the saturation temperature of the flowing fluid.
2. Particulate fouling — the accumulation of finely divided solids suspended in a process fluid onto a heat transfer surface.
3. Chemical reaction fouling — deposits formed on a heat transfer surface by chemical reactions in which the surface material itself is not a reactant.
4. Corrosion fouling — the heat transfer surface reacts to produce corrosion products which foul the surface.
5. Biological fouling — the attachment of biological organisms to a heat transfer surface along with their products.
6. Freezing fouling — solidification of a liquid or its constituents onto a subcooled heat transfer surface.

Depending on heat exchange conditions (surface temperature, water chemistry, water temperature, and flow characteristics) one or a combination of the above fouling types may occur. This study focuses on type 1, precipitation fouling or scaling.

Precipitation Fouling

The main driving force in precipitation fouling is the supersaturation level of the deposit forming species (8). Supersaturated solutions contain more than the equilibrium amount of solid in solution. Process conditions leading to supersaturation are as follows (8):

1. A solution is evaporated beyond the solubility limits of a dissolved salt.
2. A solution containing a dissolved inverse soluble salt is heated above its solubility temperature.

Inverse solubility salts become less soluble with increasing temperature. Some examples of inverse solubility salts are $CaSO_4$, $CaCO_3$, $Ca_3(PO_4)_2$, $CaSiO_3$, $Ca(OH)_2$, $Mg(OH)_2$, and $MgSiO_3$. These crystal precipitates can be hard and dense or soft and porous (8). An unsaturated salt in the bulk fluid can become supersaturated near a heat transfer surface where the thermal gradient is large. Some of these salts are added to cooling water for specific purposes while others occur naturally.

Due to a metastable region crystal growth on a transfer surface may or may not result from a supersaturated solution. Figure 1

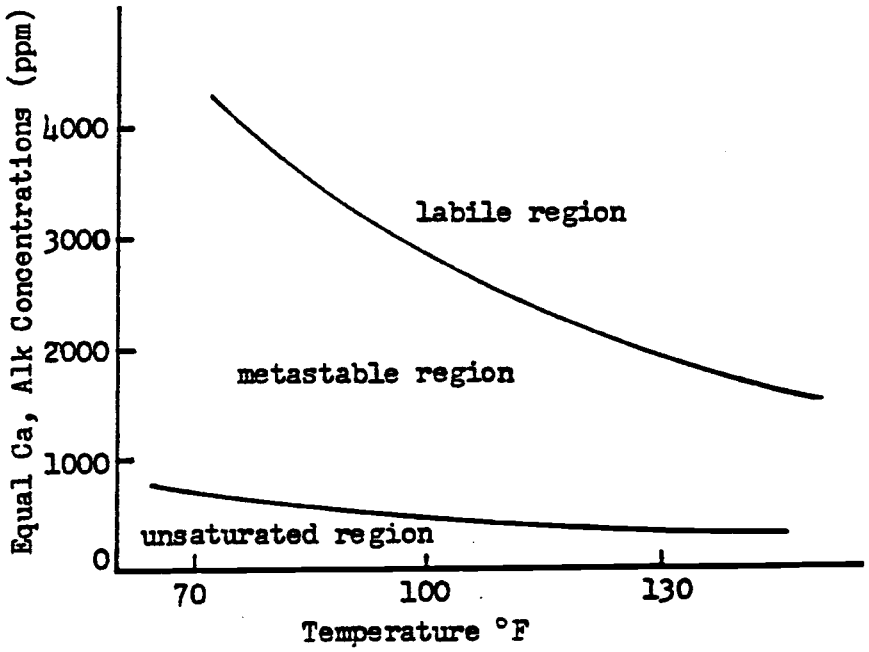

Figure 1. $CaCO_3$ Solubility Diagram

shows such a region for $CaCO_3$ (6). In the metastable region, small unstable nuclei form and dissolve without crystal growth. In the labile region larger nuclei form and crystal growth is more likely to occur. The width of the metastable region depends on the concentration of impurities and decreases with an increase in temperature (6).

Variables Affecting Scale Formation

Scale formation in a deluge dry cooling system can occur by two mechanisms (7):

1. Exceeding the solubility limit under continuous flow conditions.
2. Evaporation of the delugate on the heat exchange surface in multiple wet to dry cycles.

In continuous flow conditions the main variables of interest are water chemistry, bulk delugate temperature, surface temperature, and delugate flow characteristics. The bulk water may or may not be supersaturated with inverse solubility salts. This is greatly dependent upon water composition, temperature, and pH. Cooling water generally becomes supersaturated at higher temperatures (>60^{o}C) and pH (>7) ranges. Due to operating conditions cooling water may be supersaturated at the heat transfer surface, where temperatures are higher, but not in the bulk fluid. Surface temperature also has an effect on the reaction (attachment) rate at the heat transfer surface. An Arrhenius type equation is generally assumed to represent this effect (20). If there is rapid crystalization at the surface then mass transfer might control the deposition. A higher delugate flow rate would then enhance scale formation by increasing the convective mass transfer coefficient. However, high flow rates might also have an adverse effect on scale formation by shearing off deposits already formed on the surface (20). Flow conditions can be affected by surface geometry in such a way that scale formation will be enhanced. Past research in a corrugated finned system found deposition to be confined primarily to ridges suggesting possible nonuniform deluge flow (9, 22).

At the end of each wet cycle there will be a residual amount of delugate left on the heat transfer surface. As the surface heats up and this residual delugate evaporates, the solution will become supersaturated and salts will precipitate onto the surface. The quantity of scale formed on the surface will depend on the concentration of salts in the delugate, and how much water adheres to the surface between cycles. The amount of water adhering to the surface will depend on surface geometry and surface wettability. For example, finned tubes will hold more water between cycles than plain tubes.

The accumulative effect of continuous flow and evaporation on scale formation might lead to a net loss in scale deposited compared to the two effects taken as acting independently. This depends greatly on the number and duration of deluge cycles over a given period of time. Evaporative scale is not formed under a continuous shear and is higher in impurities. Thus, scale deposited during evaporation is less tenacious than scale deposited during continuous flow. Some of the evaporative scale could shear off during continuous flow conditions.

Net Rate of Scale Formation

The net rate of scale formation is often idealized as the difference between a deposition rate and a removal or re-entrainment rate (2):

$$\frac{dm}{d\theta} = \dot{m} = m_d - m_r \qquad (1)$$

Where:

$\dot{m}$ is the net rate of deposition per unit area;

m_d is the rate of deposition per unit area;

m_r is the rate of removal per unit area; and

θ is time.

Two limiting cases of Equation (1) are observed in experiment. If the deposition rate is constant and the removal rate is either negligible or constant, then a straight line would be generated as shown by curve A in Figure 2. In the second case the removal rate increases with the mass deposited. The deposition and removal rate ultimately become equal resulting in an asymptotic fouling, as shown by curve B in Figure 2 (20). Figure 3 shows fouling curves similar

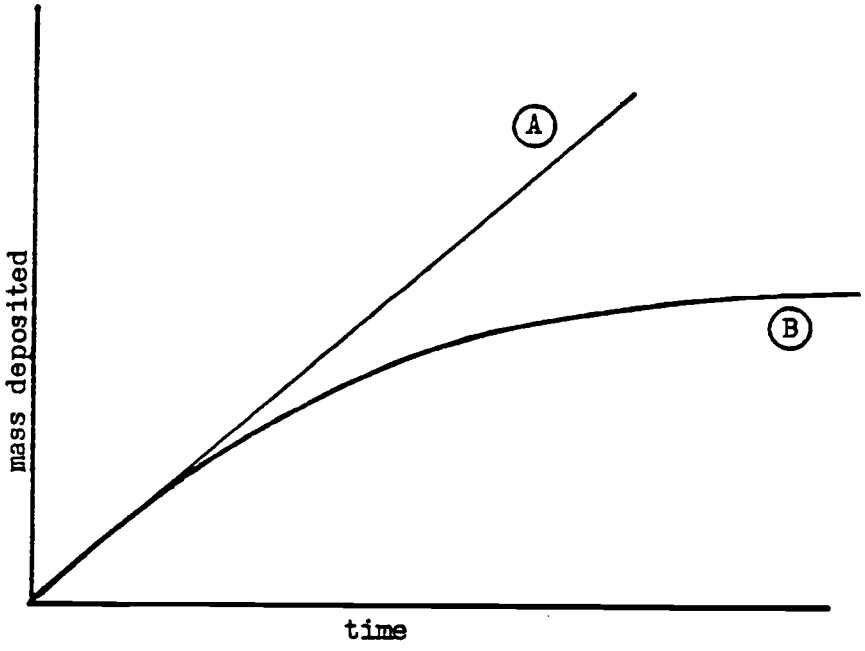

Figure 2. Typical Fouling Curves

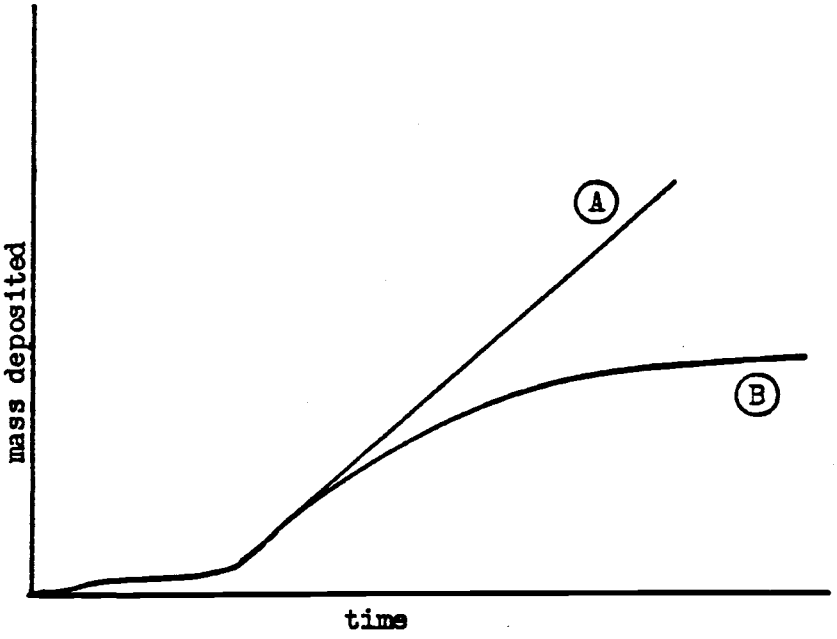

Figure 3. Fouling Curves with an Induction Period

to Figure 2 with the inclusion of an induction period preceding scale growth (20).

The second case solution to Equation (1) can be obtained by assuming the rate of deposition remains constant with respect to time, and the rate of removal is directly proportional to the mass deposited. Equation (1) now becomes:

$$\frac{dm}{d\theta} = m_d - bm \qquad (2)$$

With the initial condition of zero mass deposited at time zero, the solution to Equation (2) is:

$$m = \frac{m_d}{b} (1 - \exp(-b\theta)) = m^* (1 - \exp(-b\theta)) \quad (3)$$

where m^* is the asymptotic value reached when the deposition and removal rates are equal (see Figure 2, curve B). Equation (3) is commonly referred to as the Kern-Seaton equation (11). At large times m^* is approached and Equation (2) can be represented in its steady state form:

$$m_d = bm^* \quad (4)$$

or

$$\frac{1}{b} = \frac{m^*}{m_d} \quad (5)$$

where $\frac{1}{b}$ is the time constant of Equation (3).

Deposition Models

The deposition term in Equation (1) depends on both the transport of a species to the surface and the attachment or reaction at the surface. Epstein presented a model taking both phenomenon into account (3):

$$m_d = \frac{C_b - C_{sat}}{\frac{1}{K_m} + \frac{1}{K_r (C_s - C_{sat})^{(n-1)}}} \quad (6)$$

Where:

K_m is the mass transfer coefficient;

K_r is an n^{th} order reaction rate constant;

C_b is the bulk concentration of the precipitating species;

C_s is the surface concentration of the precipitating species; and

C_{sat} is the saturation concentration of the precipitating species.

At high flow rates K_m increases and $C_b \sim C_s$, so Equation (6) becomes:

$$m_d = K_r (C_b - C_{sat})^n \quad (7)$$

In Equation (7) the reaction rate controls the rate at which deposition will occur. For rapid reactions K_r is large. If in addition K_m is relatively small than the deposition will be diffusion controlled, with Equation (6) reducing to Equation (8).

$$m_d = K_m (C_b - C_{sat}) \quad (8)$$

Another model proposed by Taborek et al. is (20):

$$m_d = C_1 P_d (\Omega)^n \exp \left[\frac{-E}{R_g T_s} \right] \quad (9)$$

Where:

C_o is a constant;

P_d is a sticking probability factor;

Ω is a water quality factor;

E is the activation energy;

T_s is the absolute temperature at the surface; and

R_g is the ideal gas constant.

Equation (9) is based on a large amount of data collected by Heat Transfer Research Incorporated, Alhambra, California.

Epstein has presented a summary of deposition models (2). When composition, temperature, and flow conditions are constant, m_d can be assumed constant.

Removal Models

The removal of material from a heat transfer surface will involve one or more of the following phenomenon (19):

1. dissolution — material leaves in ionic form;
2. erosion — material leaves in particulate form;
3. spalling — material leaves in a large mass.

The generally accepted model for erosion, or spalling assumes the removal rate to be directly proportional to the deposit mass.

$$m_r = bm \tag{10}$$

For dissolution Burrill proposed a model of the form:

$$m_r = b_1 (C_s - C_b)m \tag{11}$$

For a system where concentration does not vary with time this equation reduces to Equation (10).

Taborek et al. proposed a removal rate equation of the form (20):

$$m_r = b_3 \tau_s m^i / \Psi \qquad (12)$$

Where:

b_3 is a constant;

τ_s is the solid shear stress;

m is the deposited mass;

i is a constant; and

Ψ is a strength factor.

Fouling Resistance

The thermal resistance on a heat transfer surface resulting from a deposited film is commonly referred to as the fouling resistance. Both direct and indirect measurements are used in the determination of fouling resistances.

Direct measurements employ thermocouples embedded directly below the heat transfer surface. When a known heat flux is applied to the surface the overall heat transfer coefficient can be calculated. If this is done for both clean and fouled conditions, the fouling resistance can be determined from Figure 4 and Equation (13) (5).

$$R_f = \frac{1}{U_f} - \frac{1}{U_c} = \left(\frac{T_{tc} - T_b}{Q/A}\right)_f - \left(\frac{T_{tc} - T_b}{Q/A}\right)_c \quad (13)$$

Where:

U_f is the overall heat transfer coefficient of the fouled surface;

U_c is the overall heat transfer coefficient of the clean surface;

Q/A is the applied heat flux;

T_{tc} is the temperature of the thermocouple embedded in the heat transfer surface; and

T_b is the bulk temperature.

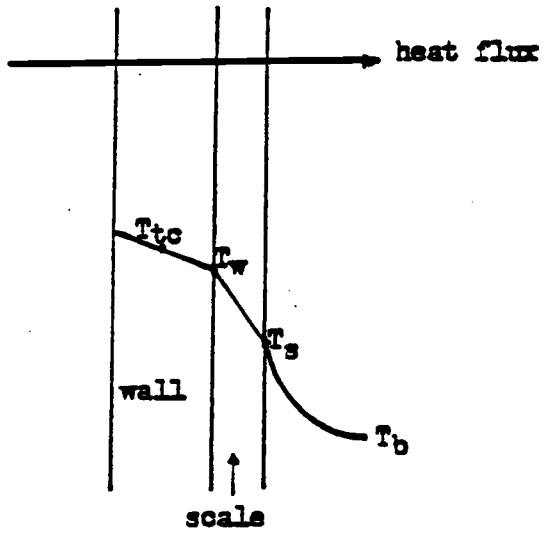

Figure 4. Temperature Profile of a Fouled Surface

Indirect measurements of fouling resistances (R_f) include thickness and mass measurements of the fouling film. These measurements can be used to approximate the fouling resistance when the overall heat transfer coefficient is difficult to measure. To approximate R_f from the mass of the film deposited Equation (14) can be used.

$$R_f = \frac{m}{\rho_f k_f} \tag{14}$$

Where ρ_f is the density and k_f is the thermal conductivity of the deposited film. A problem with Equation (14) is that the film density and thermal conductivity can vary throughout the deposit. Equation (14) assumes that the mass is deposited uniformly on the heat transfer surface.

Deluge System Models

Past research on deluge system scaling has concentrated on the measurement of mass deposited as a function of number of deluge cycles. Lin found a linear relationship for plain tubes with saturated calcium sulfate as the delugate (14). An Electric Power Research Institute (EPRI) study reported a linear relationship for a plate-tube exchanger core using well water as a delugate (22).

For an asymptotic relationship Equation (3) could be modified for a cyclic deluge system by replacing time with number of cycles:

$$m = m^* (1 - \exp(-bC)) \tag{15}$$

where C is the number of deluge cycles. Assuming the film is uniformly deposited with constant thermal conductivity and density, Equation (14) and (15) can be combined to give Equation (16).

$$R_f = R^* (1 - \exp(-bC)) \quad (16)$$

Where R^* is the asymptotic fouling resistance.

Mathematically it would be difficult to justify Equation (15) through a differential equation similar to Equation (1) because time is a continuous variable while cycles are discrete. However, Equation (15) can be used to fit data to an exponential curve in a deluged dry cooling system.

Cooling Water Characteristics

Cooling water characteristics depend a great deal on the water source, and the additives used to condition the water. Inorganic salts partly composed of calcium and magnesium occur naturally at various concentrations in cooling water. They can deposit on the surface as carbonates, sulfates, silicates, or phosphates. Corrosion inhibitors such as zinc chromate used to prevent corrosion on an exchanger surface can also form deposits. Also a fine layer of scale is sometimes used as a corrosion inhibitor (15). Polyphosphates can be used in corrosion or scale control. In the latter it is thought to distort the crystal structure of the scale making it less likely to grow (21). Such an inhibitor, in the right concentration, would reduce the fouling resistance. Some inhibitors affect the solubility curves of the other salts present. Sulfuric

acid is added to maintain the pH of cooling water between 6 and 7. Excessive corrosion can occur if the pH falls much below 6, and excessive scale deposition can occur if the pH rises much above 7 (12).

CHAPTER III

EXPERIMENTAL EQUIPMENT

The experimental equipment used in this study consisted of simulated cooling water, a simulated cooling tower, control and measurement elements, and two test sections. An overall schematic of the system is shown in Figure 5. Some of the equipment used was modified from previous studies (1, 14).

Deluge Water

Simulated cooling water was supplied from ongoing research at Oregon State University by Knudsen and Santoso (13). Continuous addition of deionized water to the system was necessary to make up for evaporative losses during the runs. Water composition was monitored at various points during the runs. In Runs 4 and 5 chemicals were added during the run in an attempt to maintain better control over the water composition. In Run 6 city water was used as a 1 pass delugate. Average water composition for each run is given in Table 1.

Deluged Dry Cooling Tower

The cooling tower consisted of a shell made of plexiglass with dimensions 0.29 x 0.29 x 1.49 m. A blower was mounted at the top of the tower to draw air up through the tower base. The tower was positioned in a water basin with its base about 2.5 cm above the water level.

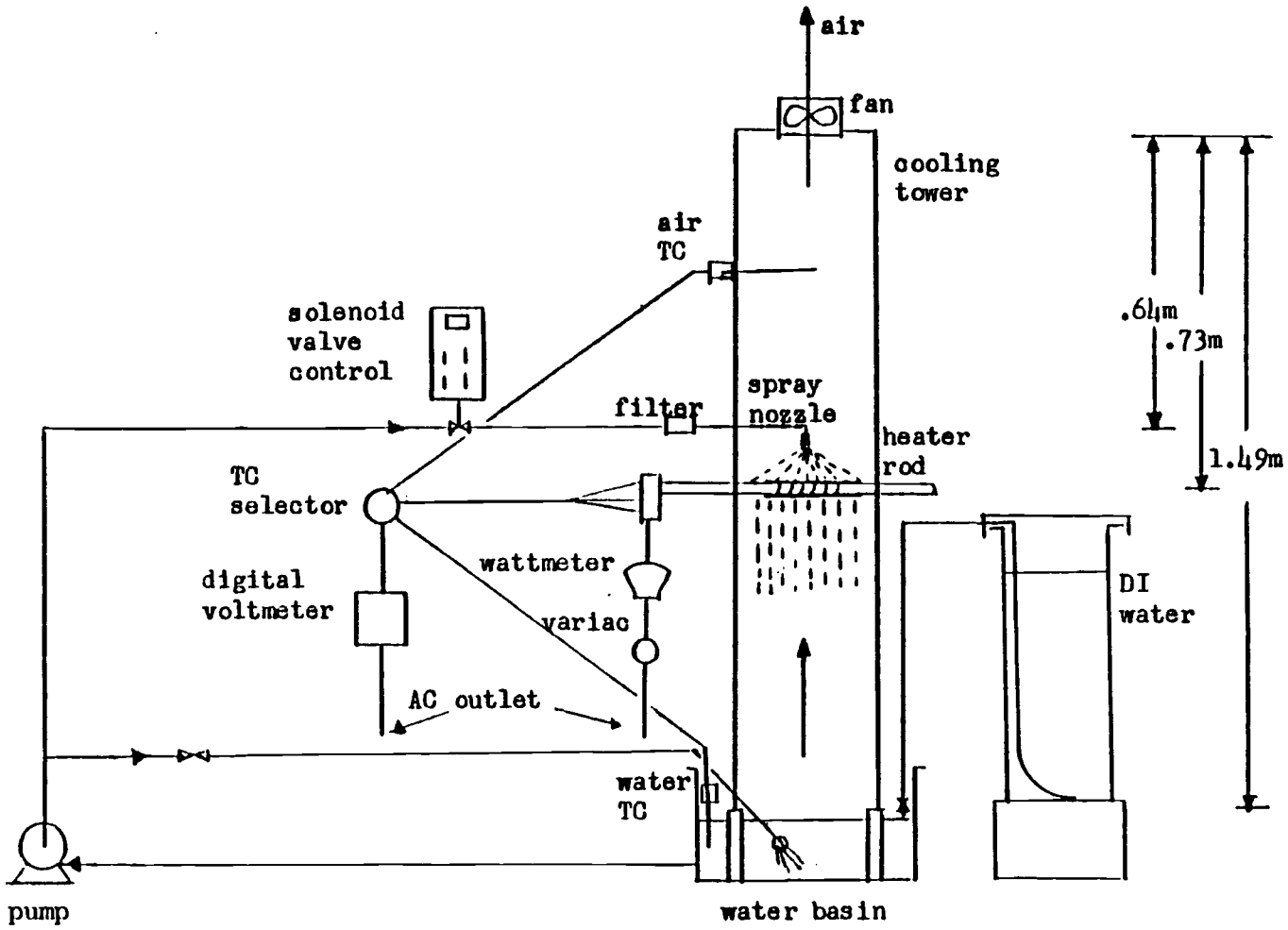

Figure 5. Schematic Diagram of Experimental Equipment.

Table 1. Average Water Conditions

	Run 1[1/]	Run 2[1/]	Run 3[2/]	Run 4[3/]	Run 5[3/]	Run 6[2/]
pH	6.0	6.5	6.84 - 6.93	6.95 (.027)	7.08 (.202)	7.51 - 7.60
T-hardness	963.0	1118.0	1125 - 1065	1245 (105)	1220 (93.5)	36.0 - 55.5
Ca-hardness	683.0	755.0	765 - 660	840 (90)	763 (26.6)	19.5 - 30.0
Mg-hardness	280.0	363.0	360 - 405	405 (15)	458 (71.3)	16.5 - 25.5
Sulfate	900.0	1100.0	1000 - 900	1050 (50)	1117 (89.8)	--
Zinc	3.0	3.9	4.4 - 3.1	3.50 (.42)	2.6 (.28)	--
Chromate	15.2	19.6	17.0 - 17.8	21.6 (.94)	20.6 (.97)	--
Silica	29.0	36.0	37 - 45	38 (119)	34 (1.0)	15 - 13
N.T.P.	1.68	4.62	.42 - .42	3.15 (1.1)	2.56 (1.03)	--
Polyphosphate	2.44	2.62	3.10 - 1.13	2.79 (1.253)	2.02 (.801)	--
Orthophosphate	7.36	6.88	8.40 - 6.52	7.81 (.750)	6.80 (.717)	--
Total Phosphate	--	--	11.50 - 7.50	12.13 (1.625)	8.88 (.375)	--
Total Inorganic Phosphate	9.8	9.5	11.50 - 7.65	10.60 (1.744)	8.82 (.298)	--
Chlorine	--	--	70 - 70	55 (5.0)	75 (5.0)	--

1/ start of run only

2/ start of run - end of run

3/ average condition (standard deviation), some chemicals added during run to maintain more constant conditions.

A heater rod used to simulate the heated surface was mounted horizontally across the tower .75 m above the tower base. The rod is made of Admiralty brass and has a 22 ohm resistance heater embedded in a section 15.2 cm long to provide the desired heat flux. Three cromel-constantin (type E) thermocouples are located just underneath the surface positioned as shown in Figure 6.

The air flow through the tower was provided by a Rotron, Inc. Tarzan axial fan. An air velocity of 1.1 m/s was measured with a Thermo Systems Inc. hot wire air velometer.

The deluge water was sprayed from a Spraying Systems Co. Unijet flat spray nozzle. The spray rate of delugate was approximately 350 ml/min for all runs. For runs 1 through 5 water was pumped from a 36.4 l basin to the nozzle where it was sprayed across the rod, and drained back into the basin. Also two by-pass streams recycled water back into the basin. For Run 6 no pump was used, instead city water was fed directly to the spray nozzle with no recycle. This modified the equipment as shown in Figure 13 (Appendix D). Teflon tubing and brass fittings were used in the flow system.

Control and Measurement Elements

The heater power was regulated by a 115 volt 5 amp variac and measured with a Jewell electric wattmeter. The thermocouples were wired through a selector switch to a digital millivoltmeter.

An R.T.C. electronic control unit connected to the water supply via an on-off solenoid valve was used to control deluge and drying

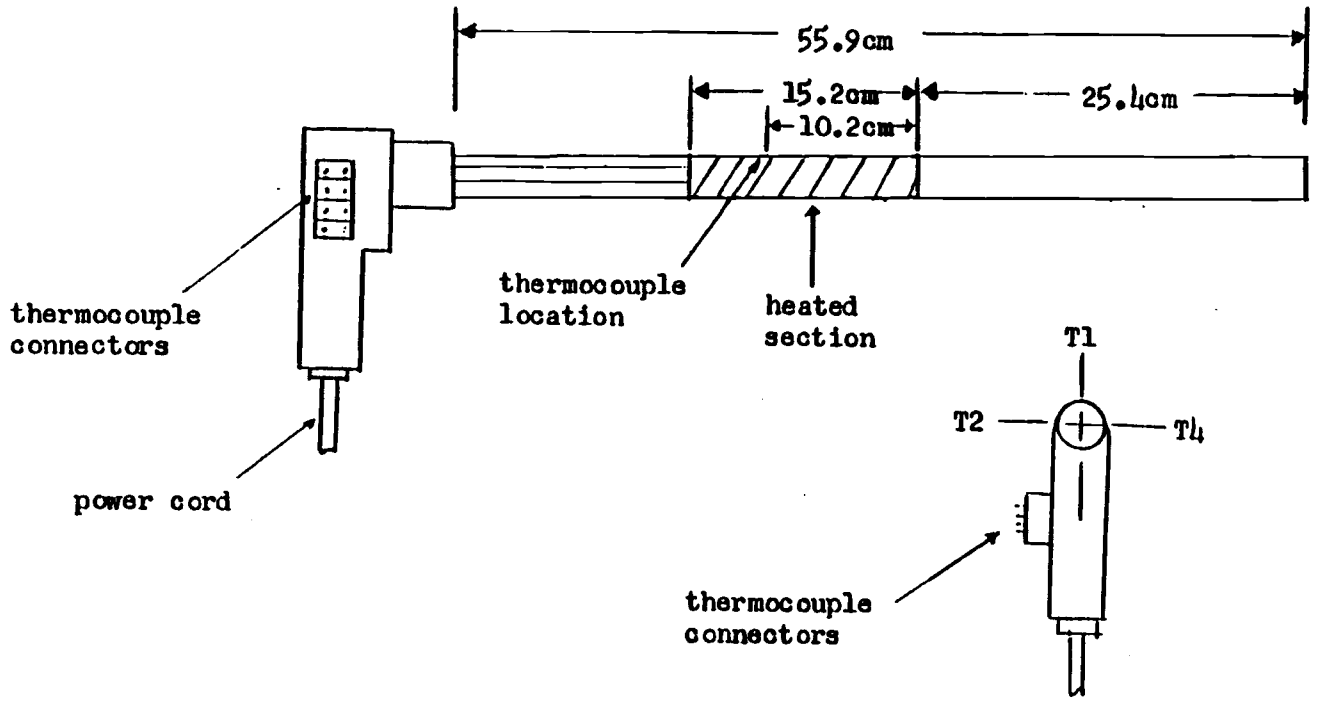

Figure 6. Heater Rod, Heated Section, and Thermocouple Locations.

times. This same unit also gave a record of the number of cycles of operation.

A Sartorius balance was used to determine the mass of the test section.

Test Sections

Two different test sections were used in this study. The test section used for Runs 1 and 2 was a plain copper alloy tube. This tube was 7.65 cm long, and 1.57 cm in outer diameter. The test section used for Runs 3 through 6 was a copper alloy transverse-helical-fin tube, with a core diameter of 1.58 cm, and 7.62 cm in length. This tube had an outside fin diameter of 1.9 cm, and there were 19 fins per inch. This tube was provided by Wieland-Werke AG Metallwerke, Postfach 42, 40 D 7900, Ulm, West Germany.

Both tubes were designed to fit with slight frictional resistance over the heater rod. The test section was slid to a position centered over the resistance heater. Also circular positioning of the test section did not vary during the runs. Two copper alloy tubes were butted at each end of the test section to minimize end effects and prevent deposition on the heater rod surface. Figure 7 shows the test section configuration.

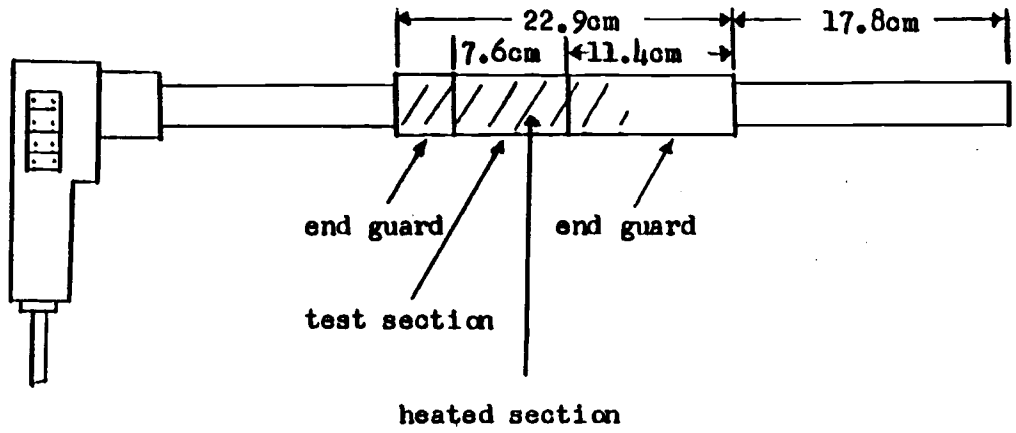

Figure 7. Heater Rod with Test Section.

CHAPTER IV

EXPERIMENTAL PROCEDURE

Six experimental runs were made in this study. A single experimental run consisted of about 1,000 cycles of operation. One cycle consisted of a 5 minute deluge period followed by 10 minutes of drying.

Before the start of each run the initial test section mass was measured. At various points during a run the test section was removed and weighed again. From the initial mass of the test section the amount of scale deposited on the test section was determined.

For Runs 1 and 2 the test section was dried on the rod with the experimental heat flux for one hour after the conclusion of a test. In Runs 3 through 6 the test section was removed from the rod and dried in an oven for one hour at $100^{o}C$. In all runs the test section was allowed to cool for about 1/2 hour before weighing.

Conditions for Runs 1 through 6 are given in Table 2.

Thermocouple temperatures were monitored and visual observations were noted periodically. Delugate samples were taken and analyzed by similar methods used by Knudsen and Santoso (13). Distilled water was added to Runs 1 through 5 when needed in order to maintain constant composition of the water. For Runs 5 and 6 chemicals were also added during the run to maintain constant water quality.

Table 2. Experimental Run Summary

Run No.	Test Section	Heat Flux	Cooling Water
1	Plain Tube	41.12 w/dm^2	Simulated
2	Plain Tube	49.34 w/dm^2	Simulated
3	Finned Tube	49.34 w/dm^2	Simulated
4	Finned Tube	57.56 w/dm^2	Simulated
5	Finned Tube	49.34 w/dm^2	Simulated
6	Finned Tube	57.56 w/dm^2	City

CHAPTER V

CALCULATIONS

Development of Best Fit Curves

All six data sets were fitted to Equations (17), (18), (19), and (20).

$$m = m^* (1 - \exp(-C/e_c)) \tag{17}$$

$$m = a_1 + b_1 C \tag{18}$$

$$\ln m = b_2 \ln C + \ln a_2 \tag{19}$$

$$m = a_3 C^{(b_3)} \tag{20}$$

Where:

m is the mass deposited per unit area;

C is the number of deluge cycles; and

m^*, e_c, a_1, b_1, a_2, b_2, a_3, b_3 are constants.

A correlation coefficient defined by Equations (21) was used to determine the best fit model for a particular run (17).

$$R^2 = \frac{\sum_i (m_i - \bar{m})^2 - SS}{\sum_i (m_i - \bar{m})^2} \tag{21}$$

Where:

$$\bar{m} = \frac{\sum_i m_i}{n} \tag{22}$$

$$SS = \sum_i (m_i - m)^2 \tag{23}$$

The best fit constants of a particular model was found by substituting the model equation into Equation (23), and minimizing the resulting equation. This method leads to linear fits for Equations (18) and (19), and nonlinear fits for Equations (17) and (20). Appendix B gives further details of the methods used.

CHAPTER VI

RESULTS AND DISCUSSION

Test Conditions

For all of the runs in this study drying and deluge times were held constant at 10 and 5 minutes, respectively. In all runs, the water flow was 350 ml/min and air velocity was 1.1 m/s across the test section. It was desired to hold the water composition constant. Unfortunately with such complex water this was a difficult task.

The average water composition for each run is given in Table 1. Water composition data is given in Appendix C. The large liquid holdup (36.4 l) in the system should have minimized the water chemistry variations. However, salts precipitating onto the tower walls and test section may be the cause of some variation.

Table 3 gives the range of parameters investigated in this study. Unavoidable changes in the ambient air temperature and humidity throughout a particular run had some effect on air, water, and rod temperatures. The small drop in temperature from the thermocouple to the test section surface was neglected, so the thermocouple temperatures are reported as the surface temperatures. Appendix E discusses this further.

Experimental Results

Table 4 presents the experimental results of the six runs in this study. Included are the number of cycles and the mass of scale

Table 3. Experimental Run Conditions

Run No.	Test Section	Total Cycles	Heat Flux w/dm^2	Average Temperature ^oC ( ) standard deviation					
				Wet Surface	Dry Surface	Wet Air	Wet Water	Dry Air	Cooling Water
1	Plain Tube	607	41.12	20.7	84.4	16.3	18.7	22.0	simulated
				(.3)	(2.2)	-	-	(1.4)	
2	Plain Tube	1,002	49.34	21.6	100.6	16.8	19.3	23.0	simulated
				(.7)	(2.8)	(.9)	(.7)	(1.2)	
3	Finned Tube	1,180	49.34	25.7	90.3	18.0	20.2	23.6	simulated
				(1.9)	(2.1)	(2.2)	(2.2)	(1.8)	
4	Finned Tube	1,061	57.56	28.3	102.6	20.5	23.5	26.7	simulated
				(.9)	(1.6)	(.8)	(.6)	(2.3)	
5	Finned Tube	1,050	49.34	27.6	91.2	20.8	21.9	25.3	simulated
				(.9)	(4.2)	(1.1)	(1.1)	(1.6)	
6	Finned Tube	1,006	57.56	24.8	103.6	21.0	18.5	25.7	city
				(.9)	(3.1)	(.3)	(1.3)	(1.7)	

Table 4. Experimental Results

Run No. 1		Run No. 2		Run No. 3	
Cycle	Mass mg/dm^2	Cycle	Mass mg/dm^2	Cycle	Mass mg/dm^2
0	0.000	0	0.000	0	0.00
90	1.087	82	0.689	97	23.30
200	5.725	270	4.346	270	43.97
380	9.355	546	8.348	505	59.77
607	11.100	762	11.560	901	80.29
		1,002	13.650	1,180	88.90

Run No. 4		Run No. 5		Run No. 6	
Cycle	Mass mg/dm^2	Cycle	Mass mg/dm^2	Cycle	Mass mg/dm^2
0	0.00	0	0.00	0	0.00
110	36.95	91	17.28	111	31.29
302	97.24	299	50.49	346	31.34
504	167.89	566	104.42	654	65.74
809	204.97	813	91.70	1,006	102.08
1,061	159.73	1,050	97.27	--	--

deposited per unit area. Raw data are given in Appendix C. Figures 8, 9, and 10 give plots of the experimental data. The curves shown on these plots will be discussed in a later section.

Figure 11 shows some test section photographs. Table 5 presents the scale analysis for Runs 3 and 4.

Discussion of Results

Experimental Runs 1 and 2

Both high and low heat fluxes gave similar results in these plain tube tests. In fact, data for the two curves did not seem to vary by more than 3 mg/dm^2. Considering the test section area (.377 dm^2) there is only about a 1.1 mg maximum difference in measured mass deposited between the two curves. With the abundance of inverse soluble salts in the cooling water the higher heat flux would be expected to deposit more mass than the lower one. Just the opposite was observed in the first 600 cycles, however, the data trends seemed to indicate that these two curves would cross in later cycles. End effects could be the cause of the discrepancy in the early cycles.

During the deluge part of the cycle the plain tube test section drained as shown:

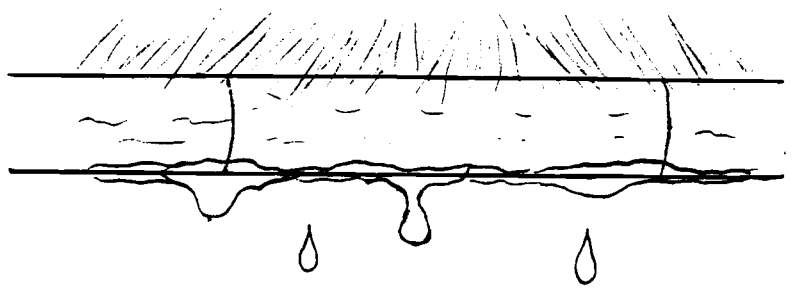

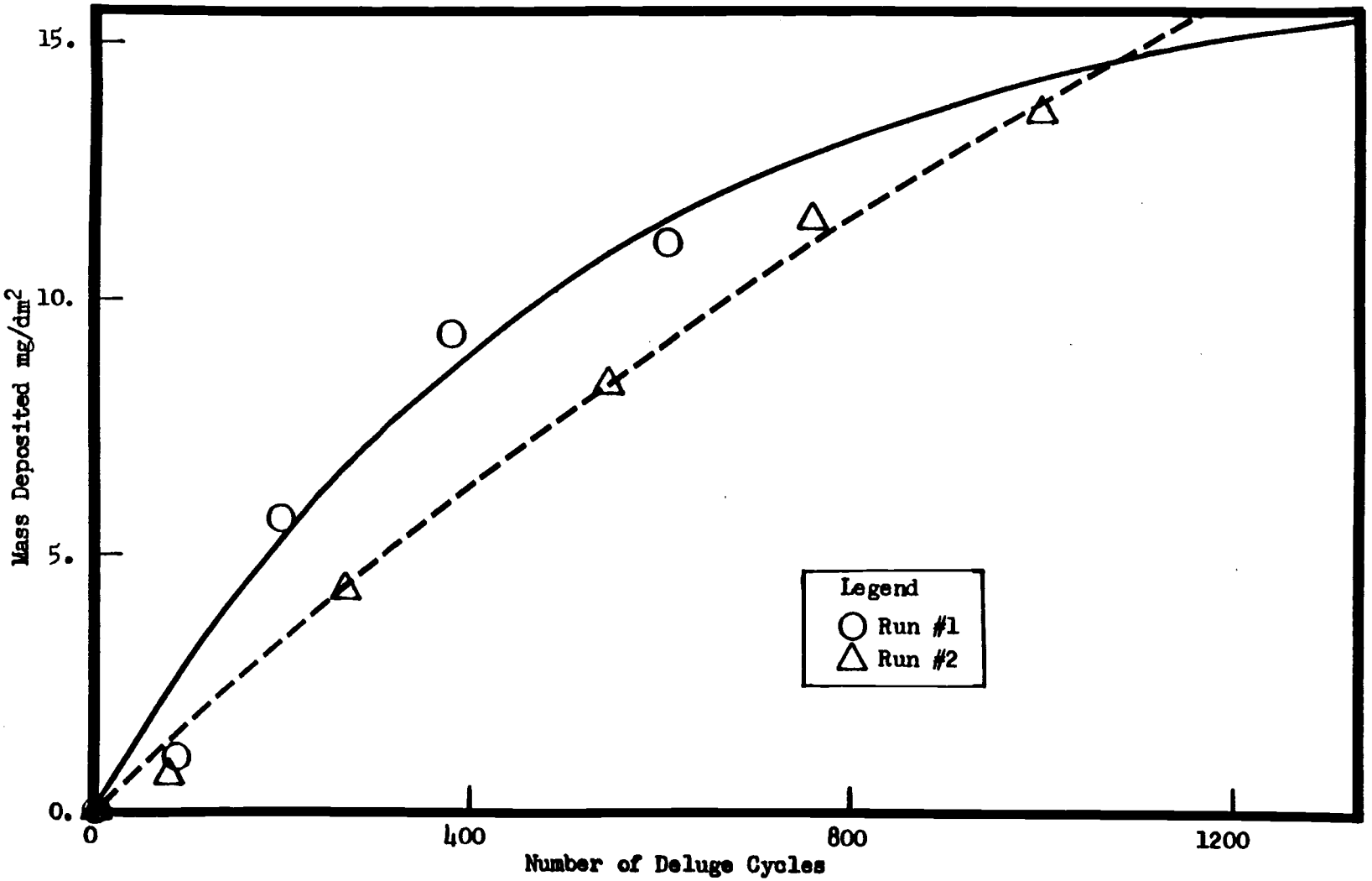

Figure 8. Mass Deposited vs. Number of Cycles, Runs 1 and 2.

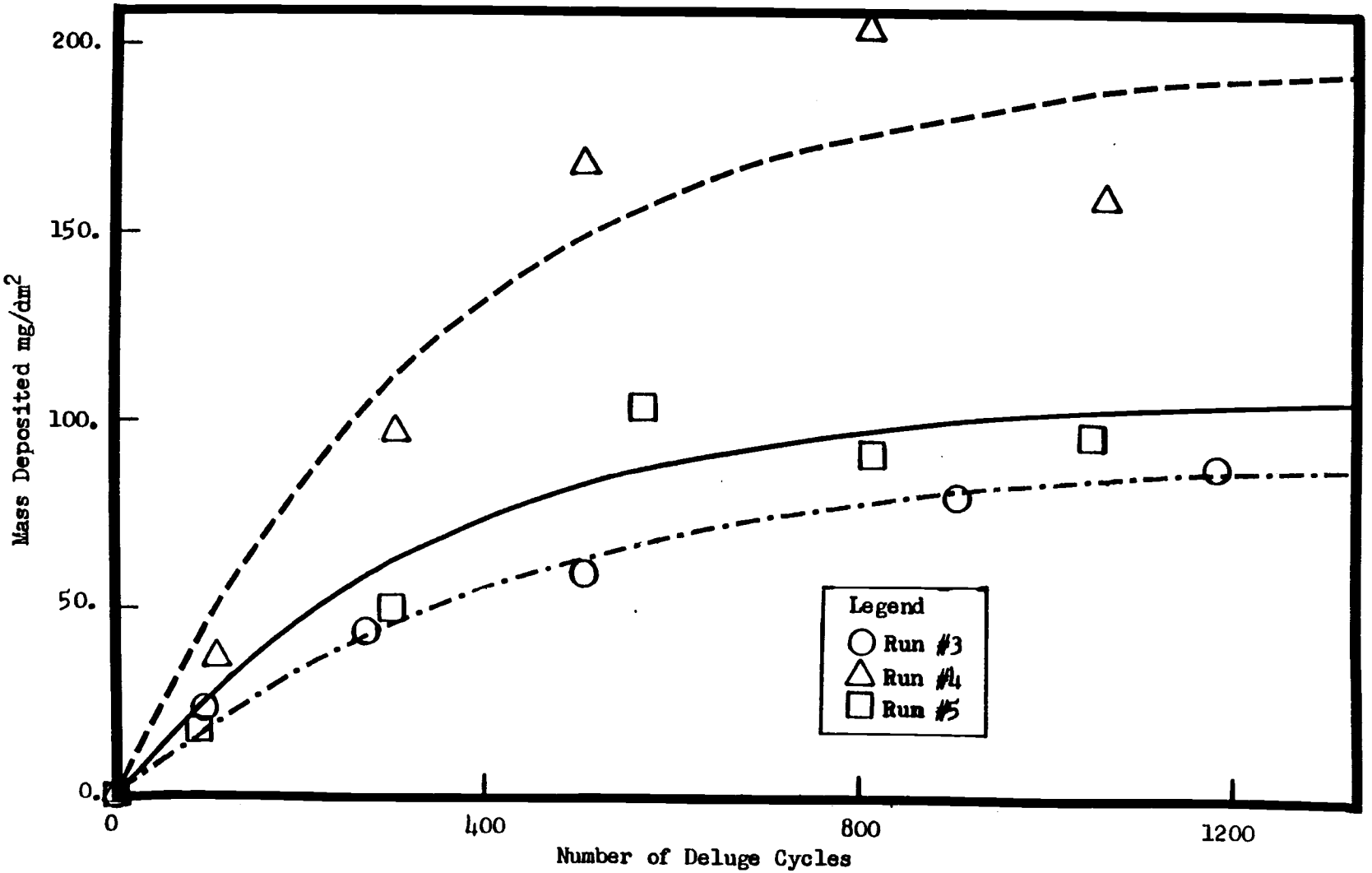

Figure 9. Mass Deposited vs. Number of Cycles, Runs 3, 4, and 5.

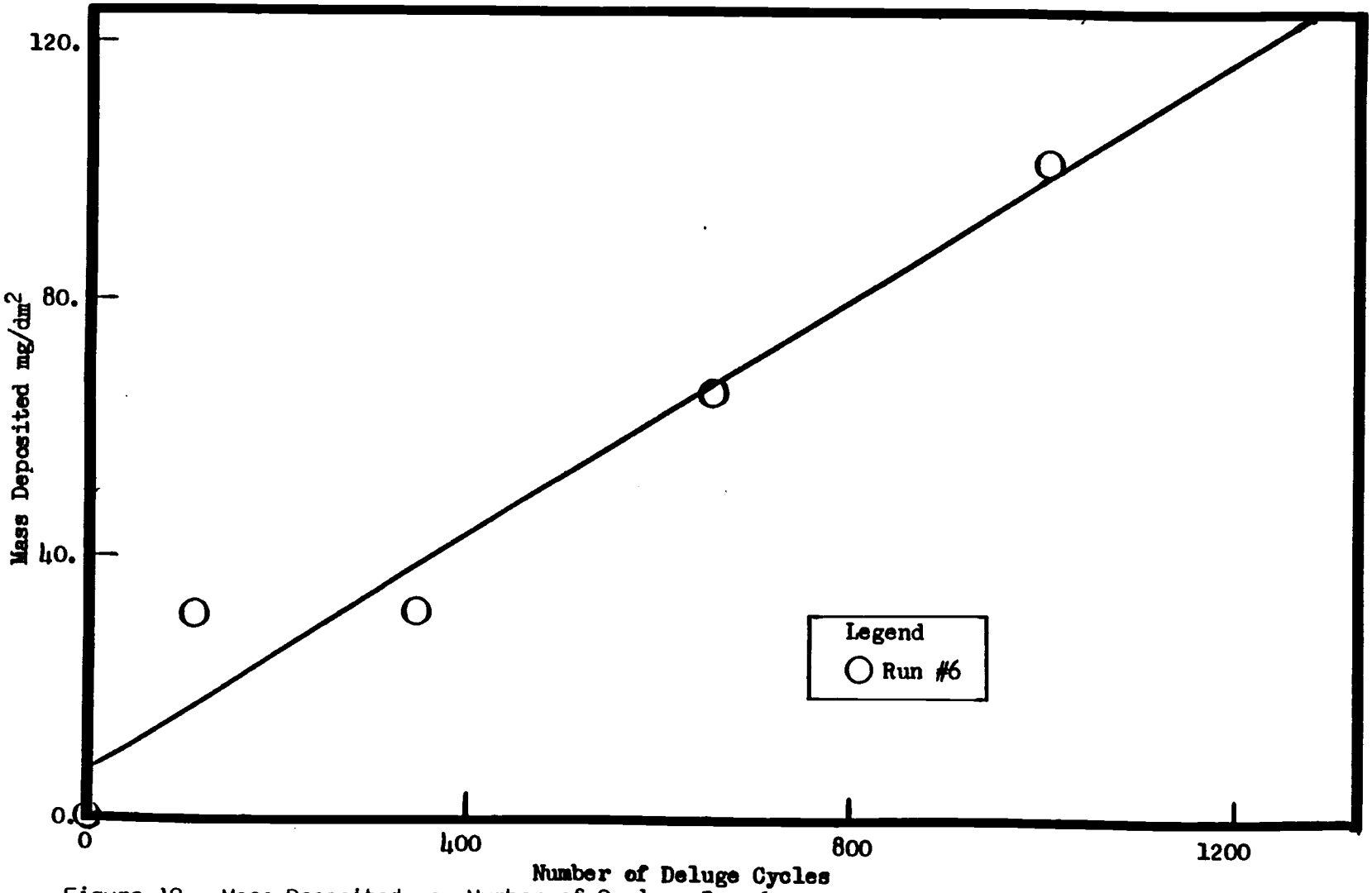

Figure 10. Mass Deposited vs. Number of Cycles, Run 6.

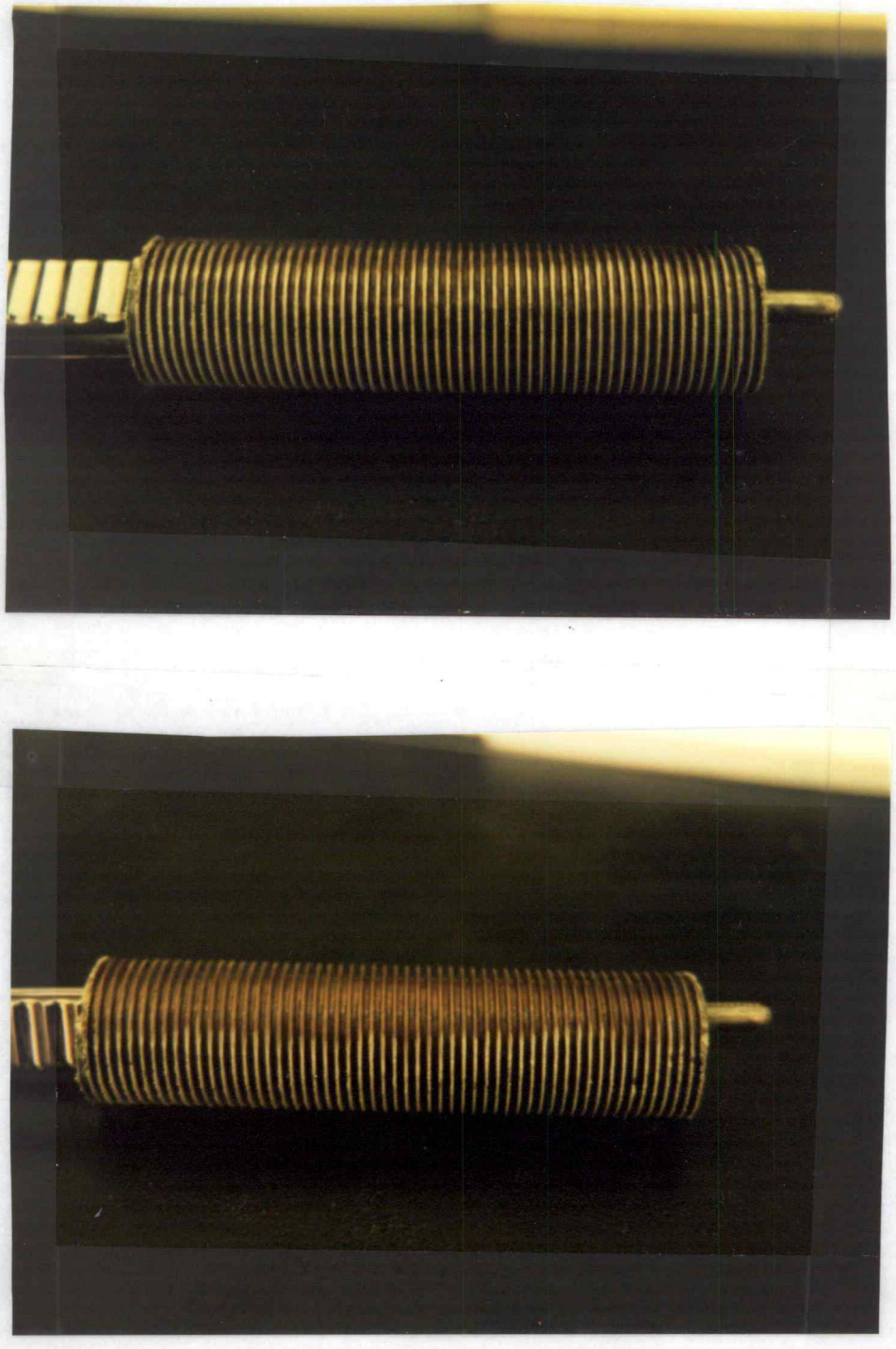

Figure 11. Test Section Photographs, End of Run 3.

Table 5. Scale Composition Runs 3 and 4 (given in percents).[1/]

	Ca	Mg	Si	Fe	Cu	Na	CO_3	SO_3	PO_4
Run #3	15.0	1.4	38.0	1.0	1.7	1.2	1.0	15.0	2.9
Run #4	20.0	1.0	26.0	1.0	2.8	1.0	1.0	14.0	2.3

[1/] The scale percentages do not add up to 100. The reason is unknown at this time. The difference could possibly be carbonate.

A thin film of liquid drained down the side of the test section and dripped off the bottom in a random fashion. At the end of each deluge cycle drops adhered to the bottom edge of the test section. These drops usually jiggled about and went to an end of the test section. Once there, either evaporation or further dripping occurred:

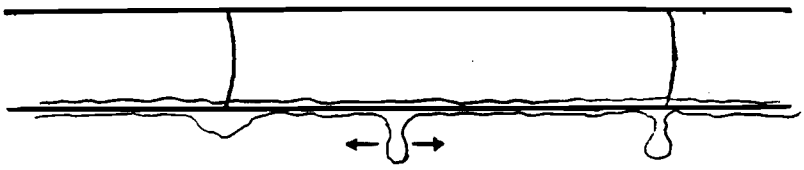

The ends of the test section where two tubes were butted together appeared to be a desirable location for water to adhere. Thus, the majority of the scale nucleation occurred at the test section ends and migrated inward. However, some scale did form along the entire lower half of test section. Near the end of the runs the scale deposit on the test section appeared as shown:

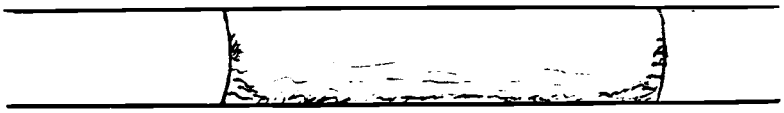

The scale was white and very tenacious.

Some scale deposited in waves. This perhaps indicates that precipitation due to evaporation occurs at the edges of the water film where higher temperatures exist. Salts in the bulk of the film diffuse to the edge where they in turn precipitate, while the film shrinks in size. Any scale deposited during the drying stage would provide a good site for salts to form on during the wetting stage of the cycle.

The top half of the test section was relatively free of scale. During the deluge part of the cycle water runs down over the top of the cylinder with relatively high shear stress. And during the drying part of the cycle water drains down off the top half before it evaporates.

To eliminate the uncertainties associated with the ends of the plain tube test section, a finned tube test section was used for Runs 3 through 6. This configuration was also studied because deluge dry cooling towers have enhanced heat transfer surfaces.

Experimental Runs 3, 4, and 5

All three of the finned tube runs generated data that appeared to be of exponential form. There was considerable variation between the high and low heat flux data. The mass of scale deposited at the higher heat flux was about twice that of the lower heat flux at the same number of cycles.

Runs 3 and 5 were run at the same heat flux and similar water chemistry. As expected the data points overall duplicated well.

The one high datum point in Run 5 occurred when, for some unknown reason, the cooling water pH went from 7 to 7.5. Other than that one instance the water pH was fairly constant at about 7 for all three runs.

During the deluge cycle the finned test section drained as shown:

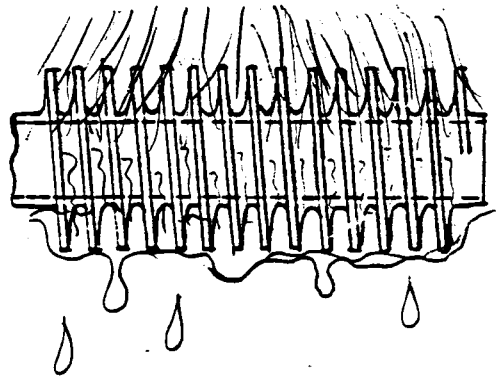

Again the cooling water dripped off the bottom of the test section in a random fashion. When the rinse ended the gaps between the fins held water on the lower half of the tube.

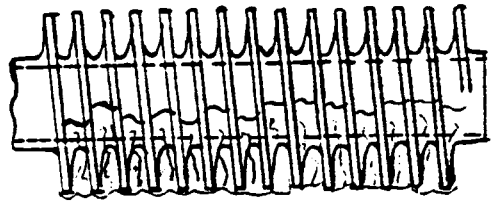

The presence of the fins eliminated all end effects.

Initial scale formation of Runs 3, 4, and 5 occurred on the ridges of the fins just below the axis as shown:

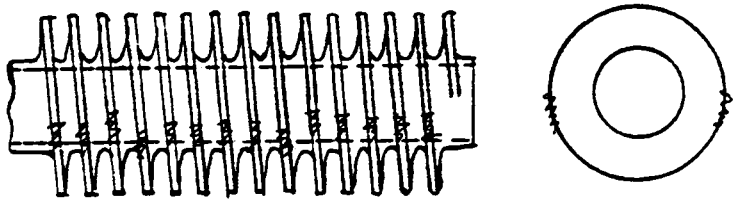

This type of scale was apparent within the first 100 cycles. At about 300 cycles a finer scale became evident on the lower fin faces and tube base. The initial scale on the fin edges grew and migrated downward along the fin ridge.

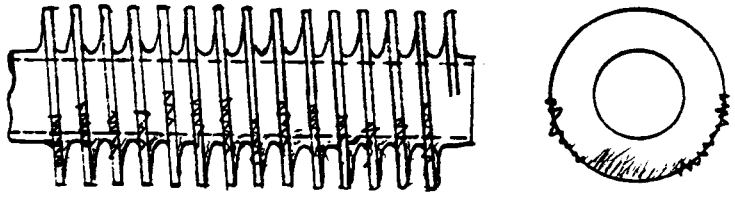

At about 600 to 800 cycles scale covered the entire lower half of the fin ridges. At the end of the runs scale was deposited on the test section as shown:

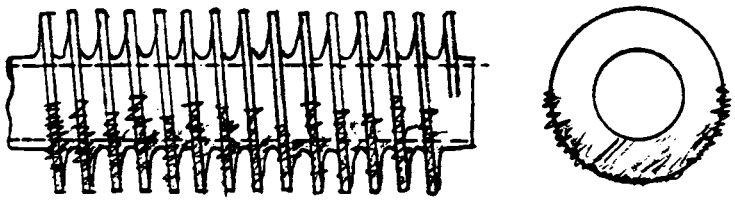

The scale on the fin tips consisted of small white crystals that decreased in size away from the horizontal axis. This scale could be scraped off easily. The lower fin faces and parts of the base tube were covered with a light fine scale that was relatively tenacious.

The scale deposits on the fin tips are probably caused by the poor flow characteristics about that portion of the test section as illustrated:

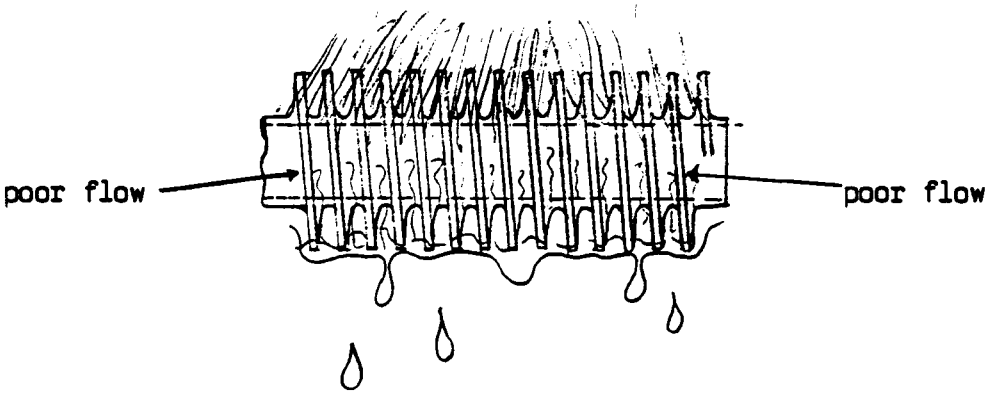

While water flows down between the fins and splatters off the top half of the tube, the fin tips just below the axis are partially dry at times. This could lead to precipitation at these points, and be a possible explanation for scale nucleation at these locations.

The scale deposits on the fin faces and lower tube base probably occurred by continuous deluge precipitation, and evaporation of residual water.

There was no scale build up on the upper half of the test section. As with the plain tube case the shear stress is relatively high at this location, and there is no residual water there when the flow is stopped.

At about 300 to 500 cycles the data implies less net mass was deposited over a given number of cycles than initially. This indicates that some type of removal mechanism becomes more effective as the deposit grows. It's this behavior that causes the data to have an exponential form (20).

Experimental Run 6

Although considerable mass accumulated on the finned test section during Run 6, very little scale was visible. Instead, a dark thin layer of corrosion was observed on the lower half of the finned test section. This build up occurred in somewhat of a linear fashion. Even though the city water pH was relatively high (7.5), the lack of corrosion inhibitors in the water coupled with the wet-dry system, could have led to conditions that promoted corrosion.

Regression Analysis

All of the data were fit to the equations previously presented:

$$m = m^* (1 - \exp(-C/\theta_c)) \tag{17}$$

$$m = a_1 + b_1 C \tag{18}$$

$$\ln m = b_2 \ln C + \ln a_2 \tag{19}$$

$$m = a_3 C^{(b_3)} \tag{20}$$

The best fit of Equations (17), (18), (19) or (20) to a particular set of data is found by varying the two parameters until a minimum value of Equation (23) is found. When Equation (19) was used, Equation (23) was modified to give the best fit in log-log coordinates.

$$SS = \sum_i (m_i - m)^2 \tag{23}$$

The methods used to find the minimum to Equation (23) are discussed in Appendix B. The correlation coefficient, Equation (21), is used as a basis to compare how well a set of data fits the model.

$$R^2 = \frac{\sum (m_i - \bar{m})^2 - SS}{\sum (m_i - \bar{m})^2} \tag{21}$$

The closer the value of R^2 to 1 the better the model fits the data (17).

Equation (17) is an exponential relation similar to Equation (3) with b replaced by $1/\theta_c$, where θ_c is a time constant. Equations (18) and (19) can be fit by linear methods, while Equations (17) and (20) have to be fit by nonlinear methods. Equations (19) and (20) give identical forms of the relationship between m and C. The difference in fit is in the fact that Equation (19) is used to give the best linear fit in log-log coordinates, while Equation (20) is used to give the best fit in normal coordinates. Equation (19) is often misused to give the best fit for Equation (20).

The calculated best fit parameters for each curve with each set of data are listed in Table 6. The last row of this table combines the data of Runs 3 and 5. Equation (17) appears to give the best overall fit for Runs 1 through 5. The only exception being Run 3 where Equation (20) has an R^2 value slightly closer to 1.

Equation (17) is plotted with the data for Runs 1 through 5 in Figures 8 and 9. The predicted asymptotic values (m^*) given by Equation (17) for Runs 1 and 2 are based on data which are not close to the asymptotic value. Runs with many more cycles would be needed to substantiate these values. In Runs 3 through 5 data were collected in the region of the asymptotic values implying that the semitheoretical Equation (17) and its m^* values are well substantiated.

As shown in Figures 8 and 9 the curves resulting from Equation (17) are similar to Curve B in Figure 2. Equation (17) assumes no induction period. Intuitively this is a good assumption because the initial evaporation of the first few cycles should provide

Table 6. Regression Analyses

Run Number	Equation 17	Equation 18	Equation 19	Equation 20
1	R^2 = .9661 m^* = 16.76 θ_c = 525.0	R^2 = .9274 a_1 = .4799 b_1 = .01948	R^2 = .8917 a_2 = .07033 b_2 = .7741	R^2 = .9440 m_3 = .04691 b_3 = .8669
2	R^2 = .9954 m^* = 37.79 θ_c = 2185.0	R^2 = .9900 a_1 = .1005 b_1 = .01427	R^2 = .8888 a_2 = .05713 b_2 = .7602	R^2 = .9914 a_3 = .07156 b_3 = .9704
3	R^2 = .9922 m^* = 93.27 θ_c = 440.7	R^2 = .9137 a_1 = 15.150 b_1 = .06963	R^2 = .6235 a_2 = .2609 b_2 = .8765	R^2 = .9943 a_3 = 1.731 b_3 = .5627
4	R^2 = .9270 m^* = 198.5 θ_c = 362.4	R^2 = .7548 a_1 = 32.04 b_1 = .1703	R^2 = .6260 a_2 = .4250 b_2 = .9225	R^2 = .8565 a_3 = 2.950 b_3 = .6094
5	R^2 = .9436 m^* = 108.4 θ_c = 374.6	R^2 = .8089 a_1 = 14.82 b_1 = .0966	R^2 = .7521 a_2 = .2823 b_2 = .8875	R^2 = .8892 a_3 = 1.372 b_3 = .6330
6	R^2 = .9336 m^* = 437.3 θ_c = 3,856.4	R^2 = .9488 a_1 = 6.956 b_1 = .09243	R^2 = .8962 a_2 = .2599 b_2 = .8782	R^2 = .9308 a_3 = 1.087 b_3 = .6434
3 and 5	R^2 = .9271 m^* = 99.65 θ_c = 386.9	R^2 = .7992 a_1 = 15.79 b_1 = .01807	R^2 = .6589 a_2 = .2714 b_2 = .8820	R^2 = .8886 a_3 = 1.632 b_3 = .5895

nucleation sites for further scale to form.

In Run 6 Equation (18) gives the best fit line through the data. This equation is plotted with the data in Figure 10.

The data of Run 4 is used to show how the various models fit the data. The results are shown in Figure 12.

The parameters of Equation (17) have some physical significance. The time constant θ_c is related to the removal rate proportionality constant used in Equation (12), by Equation (24):

$$\theta_c = \frac{1}{b} \tag{24}$$

At constant composition b is thought to be mainly dependent upon flow velocity and geometry. Hence, the values of b for Runs 3, 4, and 5 should not vary greatly from each other. Table 7 shows that the values of b and θ_c are reasonably close together.

Using the average value of θ_c and Equation (17), a prediction of the number of cycles needed to reach 95 percent of the asymptotic mass deposited can be made:

$$\frac{m}{m^*} = .95 = 1 - \exp(-C/\theta_c) \tag{25}$$

Equation (25) gives 1,180 cycles required to reach 95 percent of the asymptotic value. This number is very dependent on flow velocity, flow geometry, and water composition.

Knowing the values of b and m^* also enables the calculation of m_d, the deposition rate. Using Equation (4) this value is also

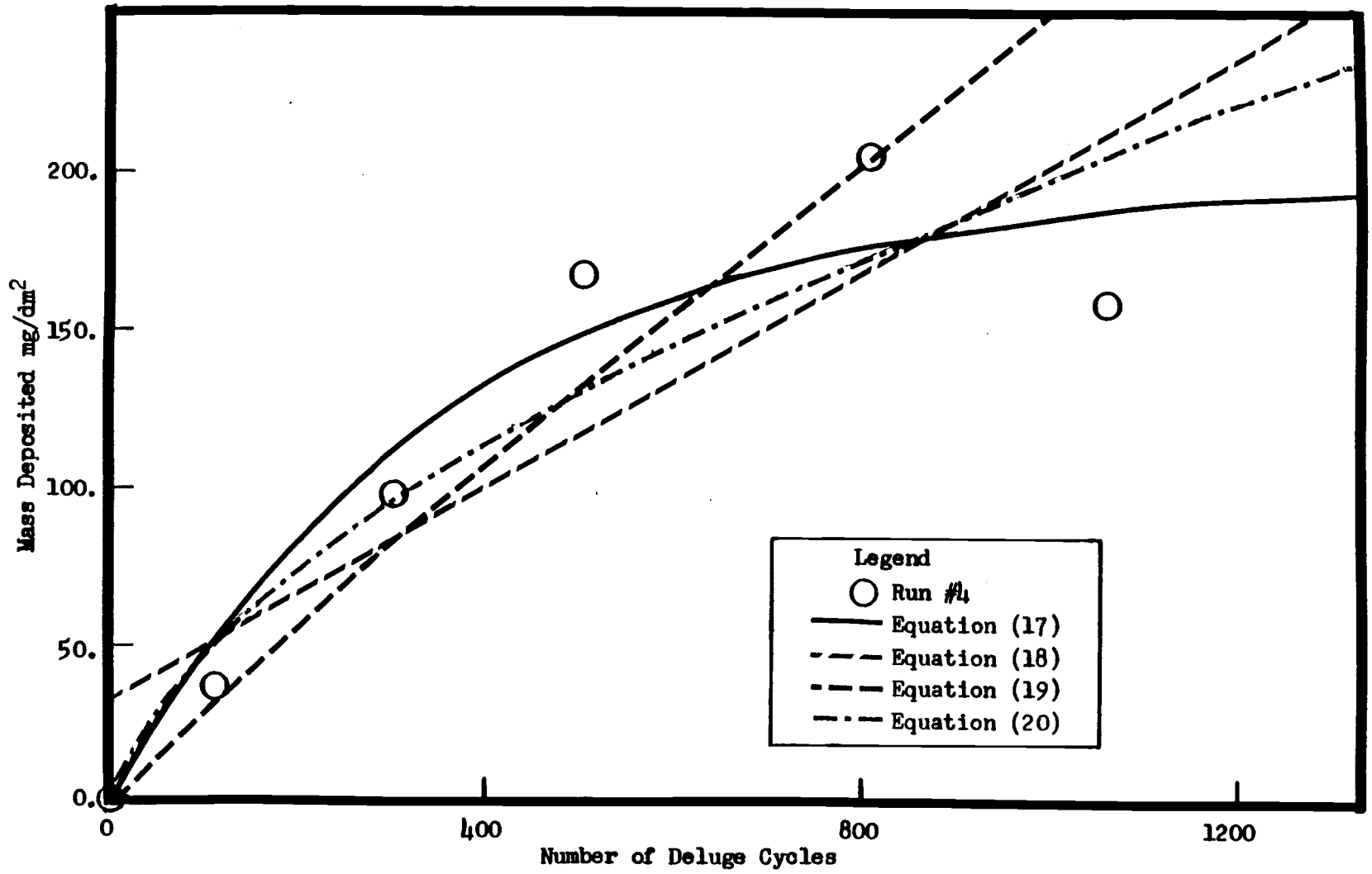

Figure 12. Best Fit Curves for Run 4.

Table 7. Comparison of Curve Parameters

Run Number	e_c	b	m^*	m_d
3	440.7	.00227	93.27	.212
4	362.4	.00276	198.45	.548
5	374.6	.00267	108.65	.289
average	392.6	.00255	—	—

tabulated in Table 7. The deposition rate should be a function of surface temperature, water composition, and flow rate. With composition and flow rates fairly constant, the similar values of m_d for Runs 3 and 5 are as expected. The larger value of m_d for Run 4 is also expected. The value of m_d also represents the initial slope of the curves. This can be shown by taking the limit of Equation (2) as θ approaches zero.

$$\left.\frac{dm}{d\theta}\right|_{\theta \to 0} = m_d \tag{26}$$

Comparison of Plain and Finned Tube Runs

Figures 8 and 9, show that considerably more mass per unit area was deposited on the finned test section than on the plain tube. This suggests that the finned tube augments scaling as well as heat transfer. However, much of the scale deposited on the finned tube was confined primarily to the fin ridges. This type of scale formation has been previously reported, and thought to suggest that nonuniform deluge flow occurs on finned tubes (9, 22).

A comparison of temperature data for Runs 2 (plain tube) and 3 (finned tube) further indicate the existence of nonuniform flow about the finned tube test section. The heat flux of 49.3 w/dm^2 was the same for both runs, and bulk air and water temperatures were similar. The average dry surface temperature of the finned tube was about $10^{o}C$ less than that of the plain tube as expected because of the higher rate of heat transfer from the finned tube. However,

during deluging the average surface temperature of the finned tube was about $4^{o}C$ greater than that of the plain tube. This suggests that the extended surface is not wetted as uniformly as in the case of the plain tube. A short discussion given in Appendix D further validates this observation.

Results from Literature

Very little actual data for scaling in deluged dry systems could be found in the literature. None could be found with similar cooling water. Barton observed some fouling curves with falling rates in her study (1). She used softer water with few additives. Lin observed a linear relationship between mass deposit and number of cycles in his study (14). He used a saturated calcium sulfate solution as a delugate. Both studies used a plain tube test section.

Using concentrated well water as a delugate Wheeler et al. studied scaling in a deluged dry system. They found the scale deposition on the heat exchanger core to be linearly dependent upon the number of deluge cycles. Using an exchanger core their data includes effects from localized hot spots and splattering.

Scale Prevention

Generally some type of enhanced heat transfer surface is needed in air cooled systems. In this study the finned test section had about 3.6 times the area per unit length of the plain test section. This has obvious advantages. One way to prevent scale build up due

to nonuniform deluge flow might be to spray the finned sections from the side as well as the top of the tubes. This would put a direct shear on the fin ridges where crystals start to grow. Another method to reduce scale build up in a deluge system would be to rinse the exchanger surface with deionized water between cycles (22).

If scaling is confined to fin ridges then little deterioration of heat transfer is expected. However, if the spaces between the fins becomes clogged heat transfer rates will be significantly reduced. Additives, such as commercial antiscalants or dispersants may be helpful in producing a scale that is porous and fluffy and hence, if formed, is easily removed form the surface.

CHAPTER VII

CONCLUSIONS

The fouling tendencies of a deluged dry cooling system were studied for plain tube and finned tube surfaces. Cycle times, water flow and air velocity were held constant for all runs. Variable run conditions were heat flux and cooling water type. Conclusions are based upon the operating conditions of this study. By using a heater rod with a removable test section previous difficulties of measuring small amounts of deposit (14) were eliminated.

Data and observations suggest that scale forms in both the wetting and evaporative parts of the deluge cycle. Almost all of the scale deposited on the lower half of the horizontal cylindrical heater. The rate of scaling of the finned tube test section appeared to be greater than that of the plain tube test section.

The finned tube data follows an exponential fouling curve. From the finned tube studies it can be concluded that a higher heat flux leads to a greater deposition rate, and greater asymptotic value of mass deposited. Surface geometry plays an important role in the location and rate of scale formation. Data and observations imply nonuniform flow about finned tubes.

The plain tube studies suggest an asymptotic deposit might be reached, but more data are needed to substantiate this observation.

The data were fitted to four different equations. The best fit for Runs 1 through 5 was found to be a modified form of the

Kern-Seaton deposition removal equation. Correlation coefficients varied from .927 to .995 with this model.

When city water was used as a delugate, corrosion occurred in what seemed to be a linear fashion over the range of cycles tested. In this case corrosion products appeared to constitute the major components of the deposit.

CHAPTER VIII

SUGGESTIONS FOR FUTURE WORK

The effects of deluge and drying times should be evaluated. It would be informative to look at very short deluge times to predict evaporative scaling effects, and continuous deluge data to predict sensible heat scaling effects.

The asymptotic deposition on finned tubes should be studied further. More data at various concentrations and heat fluxes would enable the evaluation of temperature and concentration dependencies.

BIBLIOGRAPHY

1. Barton, K.P., "Calcium Carbonate Scaling in a Deluged Dry Cooling System," M.S. Thesis, Oregon State University, 1982.

2. Epstein, N., "Fouling in Heat Exchangers," Fouling of Heat Transfer Equipment: Proceedings of An International Conference, Hemisphere Publishing, New York, 1981.

3. _____, "Fouling of heat Exchangers," Dubrovnik, 1981.

4. _____, "Fouling: Technical Aspects (Afterword to Fouling in Heat Exchangers)," Fouling of Heat Transfer Equipment: Proceedings of An International Conference, Hemisphere Publishing, New York, 1981.

5. Fischer, P., Suitor, J.W., and Ritter, R.B., "Fouling Measurement Techniques," Chemical Engineering Progress, 71(7), pp. 66-69, 1975.

6. Feitler, H, "Cooling Water Scale Control: The Scale Meter and the Critical pH of Scaling," Materials Protection and Performance, 11(6), pp. 29-33, 1972.

7. Fricke, H.D., and McIlroy, K., "Heat Transfer Characteristics of a Dry and Wet/Dry Advanced Condenser for Cooling Towers, EPRI-CS-2476, 1982.

8. Hasson, D, "Precipitation Fouling," Fouling of Heat Transfer Equipment: Proceedings of an International Conference, Hemisphere Publishing, New York, 1981.

9. Johnson, B.M., "Development of An Advanced Concept of Dry/Wet Cooling of Power-Generating Plants," Interim Report, EPRI-CS-1668, 1981.

10. Kern, D.Q., Process Heat Transfer, McGraw-Hill Book Company, 1950.

11. Kern, D.Q., and Seaton, R.E., "Surface Fouling - How to Calculate Limits," Chemical Engineering Progress 55(6), pp. 71-73, 1959.

12. Knudsen, J.G., "Fouling of heat Exchangers: Are We Solving the Problem?" Chemical Engineering Progress 80(2), pp. 63-69, 1984.

13. _____, "The Effects of Corrosion Inhibitors on the Fouling Characteristics of Cooling Tower Water," Progress Report No. 4 to Heat Transfer Research, Inc., December 1984. Department of Chemical Engineering, Oregon State University 97331.

14. Lin, A.F., "Mineral Scaling In a Deluged Dry Cooling System," M.S. Project, Oregon State University, 1983.

15. McCoy, J.W., The Chemical Treatment of Cooling Water, Chemical Publishing Co., 1983.

16. Morse, R.W., "Alkalinity Effects on the Scaling of Simulated Cooling Tower Water," M.S. Thesis, Oregon State University, 1976.

17. Neter, J., and Wasserman, W., Applied Linear Statistical Models, Richard D. Irwin, Inc., 1974.

18. Pratt, D.R., "Scale Formation in Deluged Dry Cooling Systems," Battelle Pacific Northwest Laboratories, BNWL-2060, 1976.

19. Somerscales, E.F., "Introduction and Summary: The Fouling of Heat Transfer Equipment," Fouling of Heat Transfer Equipment: Proceedings of an International Conference, Hemisphere Publishing, New York, 1981.

20. Taborek, J. et al., "Fouling: The Major Unresolved Problem in Heat Transfer," Chemical Engineering Progress 68(2), pp. 59-67, 68(7), pp. 69-78, 1972.

21. Troup, D.H., and Richardson, J.A., "Scale Nucleation on a Heat Transer Surface and Its Prevention," Chemical Engineering Communications, 2, pp. 167-180, 1978.

22. Wheeler, K.R., et al., "Deposition and Corrosion Phenomena on Aluminum Surfaces Under Deluged Dry Cooling-Tower Conditions," EPRI-CS-1926, 1981.

23. Hewlett Packard, "Standard Applications Handbook," August 1980.

24. Total Calcium and Magnesium Hardness Test Kit, HACH Chemical Company, P.O. Box 384, Leveland, CO 80537.

25. HACH Direct Reading Colorimeter Methods Manual, 12th edition, HACH Chemical Company, Ames, Iowa, U.S.A.

APPENDICES

APPENDIX A

Nomenclature

NOMENCLATURE

Symbol	Definition
A	surface area, dm^2
a_1, a_2, a_3	constants
b, b_1, b_2, b_3, C_o	constants
C	cycles
C_b, C_s, C_{sat}	concentrations, mol/l
E	activation energy, J
ID	inside diameter, cm
exp	exponential function
k_f	thermal conductivity of foulant, $\frac{J}{s\ dm\ K}$
k_m	mass transfer coefficient, m/s
k_r	reaction rate constant
OD	outside diameter, cm
m	mass deposit per unit area, mg/dm^2
m_d	deposition rate, mg/dm^2 s
m_r	removal rate, mg/dm^2 s
$\dot{m}$	net deposit rate, mg/dm^2 s
m^*	asymptotic deposit, mg/dm^2
NTP	methylene phosphonic acid
pH	negative log of hydrogen ion activity
Q	heat flux, J
R_f	fouling resistance, s cm^2 K/J
R_g	ideal gas constant, latm/mol K
R^*	asymptotic fouling resistance, s cm^2 K/J

Symbol	Definition
R^2	correlation coefficient
SS	sum of squares
T_s, T_{tc}, T_b	temperatures
T_w	water temperature
T_a	air temperature
T_1, T_2, T_3	heater rod thermocouple temperatures
U_f, U_c	overall heat transfer coefficients

Greek Symbols

θ	time, s
θ_c	time constant
τ_s	shear stress
ρ_t	foulant density, mg/dm^3
Ω	water quality factor
Ψ	scale strength factor

APPENDIX B

Calculation Details

REGRESSION PROCEDURES

Equations (18) and (19) were fit by commonly used linear regression methods. A brief description of these methods and the fitting procedure used can be found in the HP 41 CV Standard Applications Manual (23).

Equations (17) and (20) could not be linearized so a nonlinear regression procedure adapted form Morse was used (16).

$$m = m^* (1 - \exp(-C/\theta_c)) \tag{17}$$

$$m = a_1 + b_1 C \tag{18}$$

$$\ln m = b_2 \ln C + \ln a_2 \tag{19}$$

$$m = a_3 C^{(b_3)} \tag{20}$$

The general nonlinear procedure is to minimize the sum of square differences between m_i and m. For Equation (17) the sum of square differences is:

$$SS = \sum_i (m_i - m^* (1 - \exp(-C_i/\theta_c)))^2 \tag{27}$$

To find values of m^* and θ_c which minimize this equation partial derivatives must be taken with respect to m^* and θ_c and set equal to zero.

$$\frac{\delta SS}{\delta m^*} = 0 = \sum_i m_i (1 - \exp(-C_i/\theta_c)) - m^* \sum_i (1 - \exp(-C_i/\theta_c))^2$$

or

$$m^* = \frac{\sum_i m_i \, (1 - \exp(-C_i/\theta_c))}{\sum_i (1 - \exp(-C_i/\theta_c))^2} \tag{28}$$

$$\frac{\delta SS}{\delta \theta_c} = 0 = \sum_i C_i \, m_i \exp(-C_i/\theta_c) - m^* \sum_i C_i \, ((1 - \exp(-C_i/\theta_c))$$

$$\exp(-C_i/\theta_c) \tag{29}$$

Substitute Equation (28) into Equation (29) and let $Y_i = \exp -C_i/\theta_c$:

$$0 = \sum_i C_i \, m_i \, Y_i - \frac{\sum_i m_i \, (1 - Y_i)}{\sum_i (1 - Y_i)^2} \sum_i C_i \, Y_i \, (1 - Y_i) \tag{30}$$

Equation (30) can be solved directly by iteration for θ_c. Once θ_c is found m^* can be found by Equation (28). This was done by an HP 41 CX with a math pac. The program KERN1 loads the data and calls SOLVE from the math pac ROM. SOLVE uses the program KF to find the solution to Equation (30). The programs are given at the end of this section.

The correlation coefficient (R^2) is used to compare the different equations.

$$R^2 = \frac{\sum_i (m_i - \bar{m})^2 - SS}{\sum_i (m_i - \bar{m})^2} \tag{21}$$

where

$$\bar{m} = \frac{\sum_i m_i}{n}$$

The equation that gives the R^2 value nearest to 1 is the best fit equation for a particular set of data. R^2 is only used as a means to compare Equation (17), (18), (19), and (20).

A similar method was used to find the best fit equation for Equation (20). SS now becomes:

$$SS = \sum (m_i - a_3 C_i^{b_3})^2 \tag{31}$$

Setting $\delta SS/\delta a_3$ and $\delta SS/\delta b_3$ equal to zero and combining the constant b_3 can be found by Equation (32).

$$\frac{\sum_i m_i C_i^{(b_3-1)}}{\sum_i C_i^{(2b_3-1)}} - \frac{\sum_i m_i C_i^{(b_3)}}{\sum_i C_i^{(2b_3)}} = 0 \tag{32}$$

To find a_3 use Equation (33).

$$a_3 = \frac{\sum_i m_i C_i^{(b_3)}}{\sum_i C_i^{(2b_3)}} \tag{33}$$

Equation (32) was also solved on the HP with a program similar to KERN1. The next two pages give a listing of the programs used.

```
01♦LBL "KERN1"
02 1
03 STO 12
04 0
05 STO 20
06 "N"
07 PROMPT
08 STO 10
09 21
10 +
11 STO 09
12 STO 11
13 21
14 STO 08
15♦LBL 10
16 RCL 08
17 RCL 11
18 X=Y?
19 GTO 11
20 "C"
21 PROMPT
22 STO IND 08
23 "M"
24 PROMPT
25 STO IND 09
26 ST+ 20
27 VIEW 12
28 1
29 ST+ 12
30 ST+ 08
31 ST+ 09
32 GTO 10
33♦LBL 11
34 XROM "SOLVE"
35 STO 15
36 RCL 17
37 RCL 16
38 /
39 STOP
40 STO 16
41 0
42 STO 17
43 STO 18
44 RCL 11
45 STO 09
46 21
47 STO 08
48 RCL 20
49 RCL 10
50 -
51 STO 19
52♦LBL 14
53 RCL 08
54 RCL 11
55 X=Y?
56 GTO 15
57 RCL IND 09
58 RCL 19
59 -
60 X↑2
61 ST+ 17
62 RCL IND 09
63 RCL IND 08
64 XEQ "MDEF"
65 -
66 X↑2
67 ST+ 18
68 1
69 ST+ 08
70 ST+ 09
71 GTO 14
72♦LBL 15
73 RCL 17
74 RCL 18
75 -
76 RCL 17
77 /
78 END

01♦LBL "KF"
02 STO 13
03 RCL 11
04 STO 09
05 21
06 STO 08
07 0
08 STO 16
09 STO 17
10 STO 18
11 STO 19
12♦LBL 12
13 RCL 08
14 RCL 11
15 X=Y?
16 GTO 13
17 RCL IND 08
18 RCL 13
19 /
20 CHS
21 E↑X
22 STO 15
23 RCL IND 08
24 *
25 RCL IND 09
26 *
27 ST+ 16
28 RCL 15
29 RCL 15
30 CHS
31 1
32 +
33 STO 15
34 *
35 RCL IND 08
36 *
37 ST+ 19
38 RCL 15
39 X↑2
40 ST+ 18
41 RCL 15
42 RCL IND 09
43 *
44 ST+ 17
45 1
46 ST+ 08
47 ST+ 09
48 GTO 12
49♦LBL 13
50 RCL 17
51 RCL 18
52 /
53 RCL 19
54 *
55 CHS
56 RCL 16
57 +
58 END

01♦LBL "MDEF"
02 RCL 15
03 /
04 CHS
05 E↑X
06 CHS
07 1
08 +
09 RCL 16
10 *
11 END
```

```
01♦LBL "POWER"
02 1
03 STO 12
04 0
05 STO 20
06 "N"
07 PROMPT
08 STO 10
09 21
10 +
11 STO 09
12 STO 11
13 21
14 STO 08
15♦LBL 10
16 RCL 08
17 RCL 11
18 X=Y?
19 GTO 11
20 "C"
21 PROMPT
22 STO IND 08
23 "M"
24 PROMPT
25 STO IND 09
26 ST+ 20
27 VIEW 12
28 1
29 ST+ 12
30 ST+ 08
31 ST+ 09
32 GTO 10
33♦LBL 11
34 XROM "SOLVE"
35 STO 16
36 RCL 19
37 RCL 17
38 /
39 STOP
40 STO 15
41 0
42 STO 17
43 STO 18
44 RCL 11
45 STO 09
46 21
47 STO 08
48 RCL 20
49 RCL 10
50 /
51 STO 19
52♦LBL 14
53 RCL 08
54 RCL 11
55 X=Y?
56 GTO 15
57 RCL IND 09
58 RCL 19
59 -
60 X↑2
61 ST+ 17
62 RCL IND 09
63 RCL IND 08
64 XEQ "MPOW"
65 -
66 X↑2
67 ST+ 18
68 1
69 ST+ 08
70 ST+ 09
71 GTO 14
72♦LBL 15
73 RCL 17
74 RCL 18
75 -
76 RCL 17
77 /
78 END

01♦LBL "KPOW"
02 STO 13
03 RCL 11
04 STO 09
05 21
06 STO 08
07 0
08 STO 16
09 STO 17
10 STO 18
11 STO 19
12♦LBL 12
13 RCL 08
14 RCL 11
15 X=Y?
16 GTO 13
17 RCL IND 08
18 ENTER↑
19 RCL 13
20 1
21 -
22 Y↑X
23 RCL IND 09
24 *
25 ST+ 18
26 RCL IND 08
27 ENTER↑
28 RCL 13
29 2
30 *
31 1
32 -
33 Y↑X
34 ST+ 16
35 RCL IND 08
36 ENTER↑
37 RCL 13
38 Y↑X
39 RCL IND 09
40 *
41 ST+ 19
42 RCL IND 08
43 ENTER↑
44 RCL 13
45 2
46 *
47 Y↑X
48 ST+ 17
49 1
50 ST+ 08
51 ST+ 09
52 GTO 12
53♦LBL 13
54 RCL 18
55 RCL 16
56 /
57 RCL 19
58 RCL 17
59 /
60 -
61 END

01♦LBL "MPOW"
02 ENTER↑
03 RCL 16
04 Y↑X
05 RCL 15
06 *
07 END
```

APPENDIX C

Experimental Data

Test Section Data

Plain Tube — O.D. = 1.57 cm, L = 7.65 cm

A = .377321 dm^2

Finned Tube — Fin O.D. = 1.9 cm Fin I.D. = 1.58 cm

L = 7.615 cm 19 fins/inch

A = 1.3744 dm^2

Deposition Data

Run No. 1, Plain Tube, 25 watts

Date	Cycle	Test Section Weight (g)	Scale Weight (mg)	m (mg/dm^2)
2-15	0	42.56516	0.00	0.0000
2-16	90	42.56557	0.41	1.0866
2-17	200	42.56732	2.16	5.7246
2-19	380	42.56869	3.53	9.3554
2-22	607	42.56935	4.19	11.1046

Run No. 2, Plain Tube, 30 watts

Date	Cycle	Test Section Weight (g)	Scale Weight (mg)	m (mg/dm^2)
2-27	0	42.50970	0.00	0.0000
2-28	82	42.50996	0.26	0.6891
3-2	270	42.51134	1.64	4.3464
3-5	546	42.51285	3.15	8.3483
3-7	762	42.51406	4.36	11.5552
3-10	1,002	42.51485	5.15	13.6489

Run No. 3, Finned Tube, 30 watts

Date	Cycle	Test Section Weight (g)	Scale Weight (mg)	m (mg/dm^2)
3-22	0	58.34565	0.00	0.00
3-23	97	58.37768	32.03	23.30
3-25	270	58.40608	60.43	43.97
3-28	505	58.42780	82.15	59.77
4-1	901	58.45600	110.35	80.29
4-4	1,180	58.46783	122.18	88.90

Run No. 4, Finned Tube, 35 watts

Date	Cycle	Test Section Weight (g)	Scale Weight (mg)	m (mg/dm^2)
4-9	0	58.29073	0.00	0.00
4-10	110	58.34152	50.79	36.95
4-12	302	58.42437	133.64	97.24
4-14	504	58.52148	230.64	167.89
4-17	909	58.57244	281.71	204.97
4-20	1,061	58.51026	219.53	159.73

Run No. 5, Finned Tube, 30 watts

Date	Cycle	Test Section Weight (g)	Scale Weight (mg)	m (mg/dm^2)
4-20	0	58.25675	0.00	0.00
4-21	91	58.28050	23.75	17.28
4-23	299	58.32614	69.39	50.49
4-26	566	58.40027	143.52	104.42
4-29	813	58.38278	126.03	91.70
5-1	1,050	58.39044	133.69	97.27

Run No. 6, Finned Tube, 35 watts

Date	Cycle	Test Section Weight (g)	Scale Weight (mg)	m (mg/dm^2)
5-2	0	58.19670	0.00	0.00
5-3	111	58.23970	43.00	31.29
5-6	346	58.23977	43.07	31.34
5-9	654	58.28705	90.35	65.74
5-13	1,006	58.33700	140.30	102.08

The heat flux was calculated based on the outside area of the rod above the heater (60.80 cm^2).

The temperature data of this study are given on the next two pages. Power is given in Watts, and temperatures are given in ^{o}C.

Date	Power	Cycle	Water On					Water Off				
			T_1	T_2	T_3	T_4	T_5	T_1	T_2	T_3	T_4	T_5
Run No. 1												
2-15	/25.0	0	+	+	+	+	+	87.6	88.1	22.2	87.3	23.2
2-16	/24.5	90	+	+	+	+	+	83.0	83.3	17.5	82.7	21.1
2-17	/25.0	200	+	+	+	+	+	85.0	85.2	17.5	84.3	20.4
2-19	25.5/	380	20.6	21.1	18.7	20.5	16.3	+	+	+	+	+
2-22	/25.0	607	+	+	+	+	+	82.2	82.5	19.4	82.0	23.2
Run No. 2												
2-27	/30.0	0	+	+	+	+	+	104.9	105.2	22.0	104.3	24.0
2-28	30.1/30.0	82	20.9	21.5	19.0	20.5	16.2	102.1	102.3	18.3	101.4	22.0
3-2	30.0/30.5	270	21.0	21.7	18.8	20.9	16.1	102.4	102.8	18.1	101.7	23.6
3-5	29.5/29.8	546	21.7	22.4	18.7	22.3	16.7	98.6	100.0	18.3	97.9	22.6
3-7	29.9/29.4	762	21.2	21.8	19.6	21.3	16.9	97.3	97.6	18.8	96.6	21.4
3-10	30.2/29.4	1,002	22.2	22.7	20.3	22.2	18.3	98.5	98.7	19.8	97.9	24.4
Run No. 3												
3-22	/29.0	0	+	+	+	+	+	92.0	92.4	16.4	92.3	22.3
3-23	29.6/	97	24.4	24.5	19.6	24.5	17.1	+	+	+	+	+
3-25	29.6/	270	24.3	24.4	18.9	24.5	16.7	+	+	+	+	+
3-28	30.2/	505	23.6	24.1	17.5	23.9	15.6	+	+	+	+	+
4-1	30.0/30.0	901	27.4	28.1	22.4	27.9	20.4	88.2	88.7	22.0	88.5	24.9
4-4	30.2/	1,180	27.7	28.1	22.4	28.5	20.3	+	+	+	+	+

Oate	Power	Cycle	Water On					Water Off				
			T_1	T_2	T_3	T_4	T_5	T_1	T_2	T_3	T_4	T_5
Run No. 4												
4-9	/35.0	0	+	+	+	+	+	104.3	104.7	25.9	104.6	24.8
4-10	35.0/	110	26.8	27.4	22.8	27.3	19.6	+	+	+	+	+
4-12	35.0/	302	28.7	29.1	23.5	29.1	21.5	+	+	+	+	+
4-14	35.0/34.7	504	29.0	29.4	24.5	29.6	+	102.2	102.7	24.0	102.6	29.3
4-17	34.5/	809	27.3	27.7	23.4	27.9	20.5	+	+	+	+	+
4-20	34.6/35.0	1,061	27.8	28.3	23.1	28.6	20.4	100.5	101.0	21.3	101.0	25.9
Run No. 5												
4-20	/30.0	0	+	+	+	+	+	94.7	95.2	19.0	95.1	26.4
4-21	30.0/	91	27.6	27.8	20.7	28.1	20.6	+	+	+	+	+
4-23	30.0/	299	28.1	29.5	22.9	28.8	22.3	+	+	+	+	+
4-26	30.0/30.0	566	26.1	26.5	21.2	27.0	19.7	87.1	87.7	20.4	87.4	24.1
4-29	30.0/	813	27.1	27.3	22.6	27.5	20.6	+	+	+	+	+
5-1	+	1,050	+	+	+	+	+	+	+	+	+	+
Run No. 6												
5-2	/34.6	0	+	+	+	+	+	107.3	107.9	22.3	107.9	27.7
5-3	35.0/	111	25.4	25.6	19.4	26.0	20.7	+	+	+	+	+
5-6	34.5/35.0	346	24.6	25.0	19.1	25.4	21.0	101.5	101.8	18.7	102.1	24.7
5-9	35.0/	654	23.5	23.8d	17.0	23.7	21.3	+	+	+	+	+
5-13	/35.0	1,006	+	+	+	+	+	101.0	101.5	17.6	101.3	24.8

Water Quality

pH - the cooling water pH was measured with a Beckman ϕ series pH meter.

Total hardness, calcium hardness, and magnesium hardness were all measured using the Total Calcium and Magnesium Hardness Test Kit, supplied by HACH (24).

Colorimetric methods were used in all other measurements (25). If more information is desired the reader is referred to the reference (13). The following pages contain the water data collected in this study. All measurements are given in mg/l.

	Run 1	Run 2	Run 3		Run 4				
Cycle	0	0	0	1180	0	294	400	672	809
pH	6.0	6.5	6.84	6.93	6.93	6.92	6.93	6.99	6.95
T-hardness	963	1118	1125	1065	1350	—	—	—	1140
Ca-hardness	683	755	765	660	930	—	—	—	750
Mg-hardness	280	363	360	405	420	—	—	—	390
Sulfate	900	1100	1.00	900	1100	—	—	—	1000
Zinc	3.0	3.9	4.4	3.1	4.10	—	—	3.2	3.2
Chromate	5.2	19.6	16.95	17.84	22.3	22.3	—	—	20.3
Silica	29	36	37	45	35	—	—	39	39
NTP	.68	4.62	.42	.42	4.2	—	—	—	2.1
Poly PO_4	.44	2.62	3.10	1.13	2.45	2.15	3.80	1.0	4.55
Ortho PO_4	.36	6.88	8.40	6.52	7.80	7.60	6.95	7.5	9.2
Total PO_4	*	*	11.50	7.50	10.50	—	—	—	13.75
Total Inorganic PO_4	9.8	9.5	11.50	7.65	10.25	9.75	10.75	8.5	13.75
Cl^-	*	*	70	70	50	—	—	—	60

	Run 5						Run 6	
	0	180	369	566	813	1060	0	1,006
pH	6.99	6.92	7.01	7.52	6.98	7.03	7.51	7.60
T-hardness	1200	1125	1080	1275	1335	1305	36.0	55.5
Ca-hardness	750	750	720	795	795	765	19.5	30.0
Mg-hardness	450	375	360	480	540	540	16.5	25.5
Sulfate	1000	1000	1200	1200	1200	1100	—	—
Zinc	3.0	—	2.5	2.8	2.5	2.2	—	—
Chromate	20.07	—	22.3	20.07	—	20.07	—	—
Silica	35	—	—	33	—	—	15	13
NTP	2.94	.05	2.10	4.2	—	2.52	—	—
Poly PO_4	2.25	2.25	.5	2.90	2.68	1.55	—	—
Ortho PO_4	7.00	6.75	7.90	5.6	6.32	7.20	—	—
Total PO_4	9.25	—	—	8.50	—	—	—	—
Total Inorganic PO_4	9.25	9.0	8.40	8.50	9.0	8.75	—	—
Cl^-	70	—	—	80	—	—	—	—

APPENDIX D

Efficiency Study

EFFICIENCY STUDY

Comparing wet and dry surface temperature data in Table 3, for Runs 2 and 3, leads to the conclusion that the plain tube gives better heat transfer during the deluge part of the cycle, while the finned tube gives better heat transfer during the dry part of the cycle. The conclusion is questionable because the data were taken on different days with different ambient conditions. This short study was carried out to validify the conclusion.

The same equipment and set up used in Run 6 were used in this study. Air and water flow were the same as Runs 1 through 6. Figure 13 shows the cooling tower using city water as a single pass delugate. Two runs were carried out within a 4 hour period to assure similar ambient conditions.

Temperatures were recorded for both test sections in thermal equilibrium with just air flow in the tower. Temperatures were then recorded for the surfaces after 15 minutes of deluging in the tower. The data is given in Table 8. A power input of 30 watts, giving a heat flux of 49.34 w/dm^2 was used in this study.

Once again the finned tube has a lower surface temperature in air flow, but a higher one during deluging. This implies poor flow about the finned test section relative to the plain tube test section. These values probably have considerable dependence on delugate flow rate and the type of spray nozzle used.

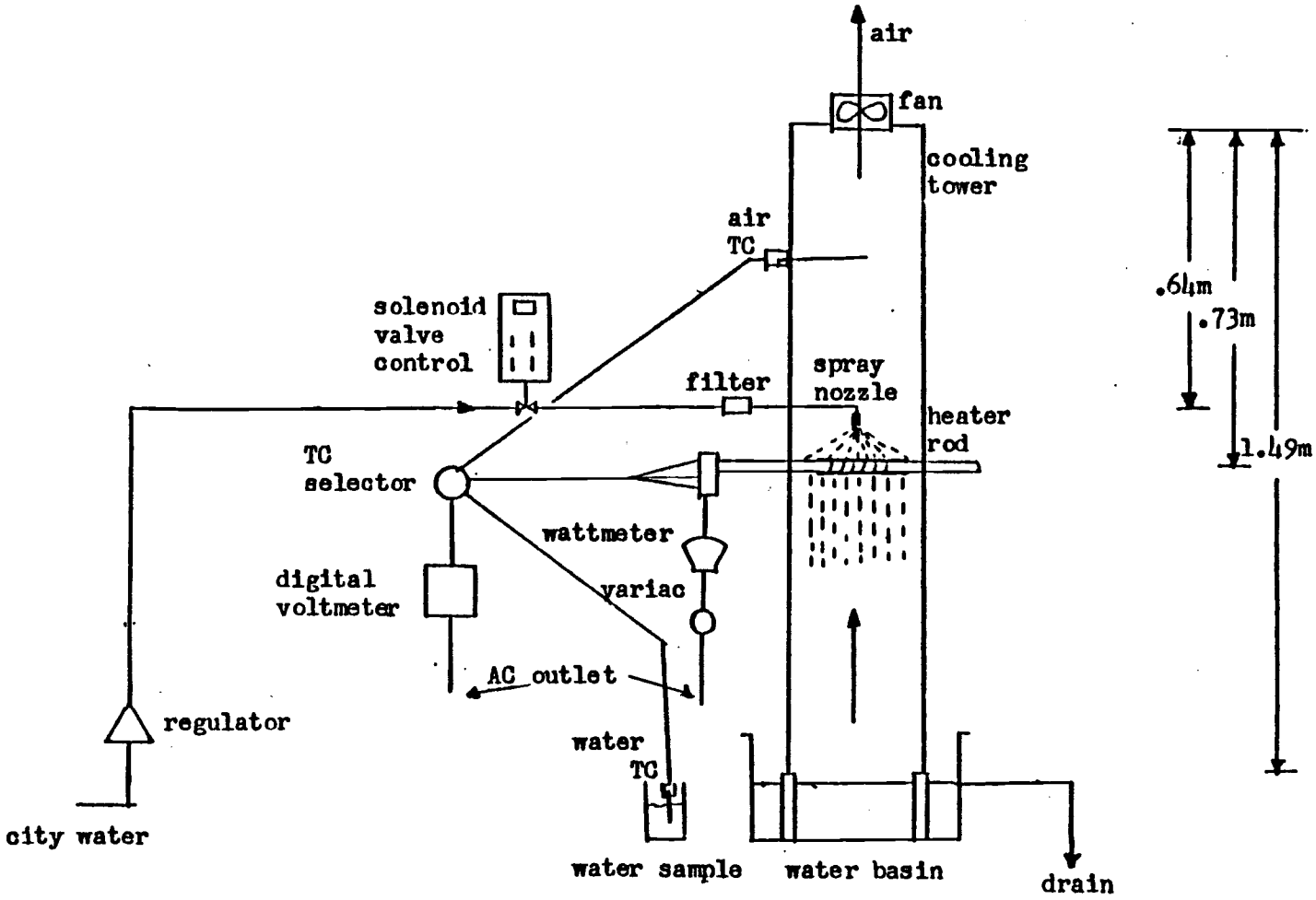

Figure 13. Schematic Diagram of Modified Experimental Equipment.

Table 8. Efficiency Study Measurements

	Water On Temperature ^{o}C					Water Off Temperature ^{o}C			
	T_1	T_2	T_4	T_{air}	T_{water}	T_1	T_2	T_4	T_{air}
Finned Tube	25.2	25.5	25.7	25.9	19.6	97.4	97.9	97.8	30.6
Plain Tube	22.0	22.5	21.2	25.0	19.6	104.6	104.7	105.0	30.7

APPENDIX E

Temperature Drop Study

TEMPERATURE DROP STUDY

The assumption has been made that the temperature drop across the test section is negligible. Calculations are presented here to justify this. First, the temperature drop between the thermocouple and the heater rod surface must be calculated. Then the temperature drop across the test section must be calculated. The resistance to heat transfer at the rod-test section interface is assumed negligible.

Knowing the heater rod thermal conductivity and the thermocouple locations enable the calculation of the rod surface temperature. Previously determined values of k/X for each thermocouple are given below (1).

Thermocouple Number	k/X
1	34625.7 Btu/hr $ft^{2o}F$
2	5091.56 Btu/hr $ft^{2o}F$
4	15232.9 Btu/hr $ft^{2o}F$

The temperature drop between the thermocouple location and the rod surface is found by Equation (34).

$$\Delta T = \frac{q}{A(k/X)} \tag{34}$$

The worst possible case would consist of the largest heat flux and the smallest k/X value. For this case (57.56 W/dm^2, thermocouple 2)

the temperature drop is .20^{o}C. This value applies to both plain and finned tube cases.

The temperature drop across the plain tube test section and the core of the finned tube test section is calculated from the following equation:

$$\Delta T = \frac{\ln\left(\frac{r_o}{r_i}\right) q}{2\pi kL} = \frac{r_i \ln\left(\frac{r_o}{r_i}\right) q}{Ak} \qquad (35)$$

For the worst possible case the largest heat flux is used. In this case the temperature drop is .02^{o}C.

There could also be a small temperature drop across the fins of the finned test section. At experimental conditions, if a value of the convective heat transfer coefficient is assumed, $h \approx 5$ Btu/hr ft^{2o}F, a fin efficiency value near 1 can be calculated (10). This means temperature variation on the fin is small.

The combined estimate of the temperature drop is .22^{o}C. This is based upon the assumption that no resistance to heat transfer exists between the rod surface and the inside of the test section.